Lasers in Medical Science (2025) 40:116
https://doi.org/10.1007/s10103-025-04315-z

REVIEW

Discussion on the comparison of Raman spectroscopy and cardiovascular disease-related imaging techniques and the future applications of Raman technology: a systematic review

Songcai Xie[1,2] · Xiaotong Zhu[3] · Feiyuan Han[1,2] · Shengyuan Wang[1,2] · Kexin Cui[1,2] · Jing Xue[1,2] · Xiangwen Xi[1,2] · Chengyu Shi[1,2] · Shuo Li[1,2] · Fan Wang[1,2] · Jinwei Tian[1,2]

Received: 24 November 2024 / Accepted: 23 January 2025

Abstract

Cardiovascular disease (CVD) is a major cause of unnatural death worldwide, so timely diagnosis of CVD is crucial for improving patient outcomes. Although the traditional diagnostic tools can locate plaque and observe inner wall of blood vessel structure, they commonly have radioactivity and cannot detect the chemical composition of the plaque accurately. Recently emerging Raman techniques can detect the plaque composition precisely, and have the advantages of being fast, high-resolution and marker-free. This makes Raman have great potential for detecting blood samples, understanding disease conditions, and real-time monitoring. This review summarizes the origin and state-of-art of Raman techniques, including the following aspects: (a) the principle and technical classification of Raman techniques; (b) the applicability of Raman techniques and its comparison with traditional diagnostic tools at different diagnosis targets; (c) the applicability of Raman spectroscopy in advanced CVD. Lastly, we highlight the possible future applications of Raman techniques in CVD diagnosis.

Keywords Raman Technsique · Spectral analysis · Cardiovascular disease · Atherosclerosis · Disease diagnosis

Abbreviations

acLDL	acetylated low-density lipoprotein
AMI	Acute myocardial infarction
BFNP	antibody-functionalized gold nanoprobe
BH4	5,6,7,8 - tetrahydrobiopterin
CARS	Coherent anti-Stokes Raman Scattering
CHD	Coronary heart disease
CK-MB	Creatine kinase-MB
CRS	Coherent Raman spectroscopy
CVD	Cardiovascular disease

✉ Fan Wang
wangfanrock@163.com

✉ Jinwei Tian
tianjinwei@hrbmu.edu.cn

Songcai Xie
2019183008@hrbmu.edu.cn

Xiaotong Zhu
m202373356@hust.edu.cn

Feiyuan Han
2018183048@hrbmu.edu.cn

Shengyuan Wang
wangshengyuanmd@163.com

Kexin Cui
918796700@qq.com

Jing Xue
xuejingsouphu@163.com

Xiangwen Xi
xixiangwen@hrbmu.edu.cn

Chengyu Shi
scy19990308@163.com

Shuo Li
dr_lisure@163.com

[1] Key Laboratory of Myocardial Ischemia, Ministry of Education, Harbin Medical University, Harbin, China

[2] Department of Cardiology, The Second Affiliated Hospital of Harbin Medical University, Harbin, China

[3] Wuhan National Laboratory for Optoelectronics, Hua zhong Univeresity of Science and Technology, Wuhan, China

Published online: 24 February 2025

CTA	Computed Tomography angiography
cTnI	cardiac troponin I
CXCR4	C-X-C Motif Chemokine Receptor 4
ECG	Electrocardiograms
18F-FDG	18 F-fluorodeoxyglucose
18F-NaF	18 F-sodium fluoride
FTIR	Fourier-transform infrared spectroscopy
H-FABP	Heart-type fatty acid-binding protein
HFPEF	Heart failure with preserved ejection fraction
ICAM-1	Intercellular adhesion molecule 1
IVUS	Intravascular Ultrasound
LSPRs	Localized surface plasmon resonances
NIRF	Near-Infrared Fluorescence
NOS	Number of spectra
miRNA	microRNA
MRI	Magnetic resonance imaging
OCT	Optical Coherence Tomography
Oro	Oil red O
OSEs	Oxidation-specific epitopes
oxLDL	oxidized low-density lipoprotein
PCI	Percutaneous coronary intervention
PDGF-BB	Platelet-derived growth factor-BB
PET	Positron Emission Tomography
RHD	Rheumatic heart disease
RMVD	Rheumatic mitral valve disease
SERDS	Shifted-Excitation Raman Difference Spectroscopy
SERS	Surface-enhanced Raman scattering
SORS	Spatially Offset Raman Spectroscopy
SRG	Stimulated Raman gain
SRL	Stimulated Raman loss
SRS	Stimulated Raman Scattering
SSTR2	Somatostatin subtype-2 receptor
TCFAs	Thin capped fibroatheromas
USPIOs	Ultrasmall paramagnetic iron oxide particles
VCAM-1	Vascular cell adhesion molecule 1

Introduction

Cardiovascular Disease (CVD) is the leading cause of death globally, accounting for nearly one-third of all disease-related fatalities [1, 2]. CVD encompasses a range of conditions that affect the heart and blood vessels [3]. In its advanced stages, CVD can only be managed to delay its progression, as complete cures are currently unavailable. Advanced CVD significantly impairs individuals' quality of life and increases the risk of mortality. Therefore, timely diagnosis of CVD is crucial for improving patient outcomes and reducing mortality rates [4].

Early CVD often manifests as mild to moderate atherosclerosis, arrhythmia, mild myocardial hypertrophy, etc., which are difficult to diagnose [5]. Among them, atherosclerosis is the main cause of CVD. Raman technique has great potential in detecting atherosclerosis [6]. We will introduce the application of Raman technique in atherosclerosis in detail later. Atherosclerosis is a chronic and progressive disease that involves the accumulation of plaque in the walls of medium and large arteries, which can reduce or block the blood flow [7]. Plaque stability depends on several factors, such as plaque composition (relative proportions of lipids, inflammatory cells, smooth muscle cells, connective tissue, and thrombus), cap fatigue from wall stress, size and location of the lipid core, and configuration of the plaque relative to blood flow [8–12]. When these factors change to abnormal state, plaque transits from stable to unstable. Unstable plaque typically contains thin fibrous caps and many macrophages with large lipid cores. As the unstable plaque progresses, it causes blood vessel luminal narrowing (<50%) and is prone to unpredictable rupture [13, 14]. The development of atherosclerosis to an advanced stage can lead to a series of CVD such as coronary artery disease, carotid artery disease, peripheral artery disease, aneurysm, etc [15].

When cardiovascular disease worsens to a certain extent, it will cause various serious diseases. Raman technique has been used to research some of them like: coronary heart disease, rheumatic heart disease, aortic aneurysm, etc. Coronary heart disease is a common and high-risk condition that is one of the main causes of heart failure. It results from a complex interplay of genetic and environmental factors [16]. The most lethal form of coronary heart disease are myocardial infarction. Myocardial infarction happens when a plaque ruptures and forms a blood clot that blocks the blood flow to the heart muscle. Rheumatic heart disease (RHD) represents a condition that may develop in individuals following an episode of rheumatic fever [17]. RHD is marked by inflammation of the heart valves, which can make them thickened and scarred, leading to stenosis or regurgitation. It is one cause of heart failure. An aortic aneurysm is a condition where the aorta develops a weak spot that bulges out like a balloon [18]. Aortic aneurysms can be congenital or acquired due to conditions such as atherosclerosis. They pose a risk due to the potential for rupture or tearing, causing massive hemorrhaging that can threaten one's life. In various cardiovascular diseases, Raman spectroscopy, taking advantage of its label-free nature, molecular specificity, and high spatial resolution, enables the quantitative and qualitative analysis of the molecular composition and structural features of pathological tissues. This capability facilitates the assessment of disease progression and associated risks. Moreover, Raman spectroscopy can detect early molecular-level alterations, thereby providing more comprehensive information for both diagnosis and follow-up.

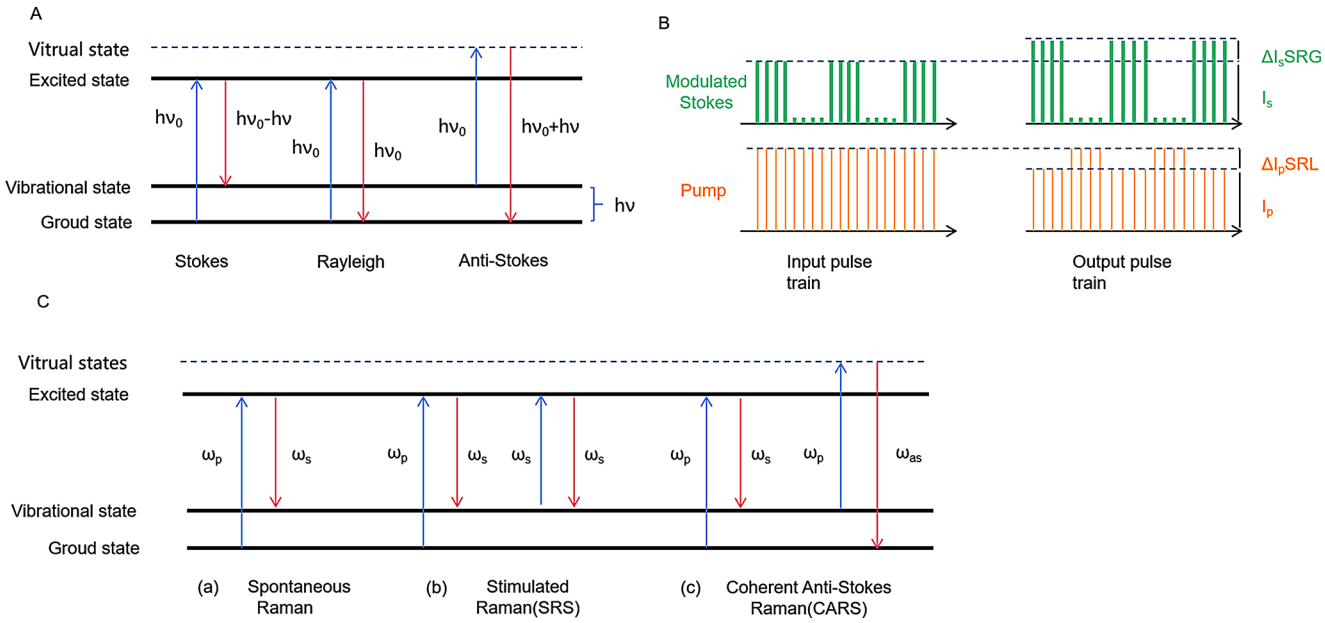

Fig. 1 Principle and comparison of Raman spectroscopy **A** Raman scattering electron level change. Stokes and Anti-stokes are specific energy changes in Raman scattering. **B** Stokes light receives energy to produce SRG signals, while pump light loses energy to produce SRL signals. **C** Energy level diagrams of spontaneous Raman scattering, SRS, and CARS processes. (a) Spontaneous Raman (b) When two laser beams with frequencies of ωp and ωs are irradiated on the sample, the frequency difference matches the molecular vibration of the sample, resulting in stimulated Raman. (c) The interaction of photons generated by two laser beams resonating with the sample with the second pump light results in a higher energy anti-Stokes light

Owing to its high sensitivity toward key proteins, lipids, and other essential biomolecules, Raman technology exhibits its significant potential in the screening and monitoring of cardiovascular conditions, thus laying a foundation for more precise interventions and treatments.

Traditionally, Computed Tomography Angiography (CTA), Positron Emission Tomography (PET), Magnetic Resonance Imaging (MRI), Near-Infrared Fluorescence (NIRF), Fourier-Transform Infrared spectroscopy (FTIR), Intravascular Ultrasound (IVUS), and Optical Coherence Tomography (OCT) have served as the imaging diagnosis tools of CVD [19]. CTA is a non-invasive method that uses contrast media and X-ray to generate three-dimensional images of blood vessels. It can detect vascular stenosis, aneurysm and other abnormalities [20]. PET is a nuclear medicine examination, which can detect myocardial ischemia, myocardial infarction and other heart diseases [21]. It uses radioactive drugs to mark specific molecules in the body, and uses a dedicated camera to generate images. MRI is a non-invasive method that uses magnetic fields and radio waves to generate images. It can detect the structure and function of cardiac muscle and blood vessels [22]. NIRF and FTIR are non-invasive imaging techniques that can provide molecular and chemical information about the sample. NIRF uses near-infrared light to excite fluorescent probes in the sample, and the emitted fluorescence is captured to generate images. This technique can provide information about the distribution of specific molecules in the sample, but its spatial resolution is relatively low. FTIR is a spectroscopic technique that uses infrared light to probe the vibrational modes of molecules in the sample. FTIR can provide quantitative and qualitative information on the biochemical content and distribution of the plaque components. IVUS and OCT are invasive examinations that can detect coronary atherosclerosis and other vascular abnormalities [23]. IVUS uses ultrasound technology to generate cross-sectional images of the coronary arteries, providing detailed information about the vessel wall and plaque characteristics. OCT uses light waves to produce high-resolution images of the structure of blood vessels, allowing for the detection of early-stage atherosclerosis and other vascular diseases. These approaches have several major limitations: (1) Insufficient spatial resolution. Due to the inherent constraints of imaging devices, these methods often fail to achieve sub-millimeter or even micrometer-level resolution; (2) Inability to directly obtain chemical composition information. Most conventional imaging techniques rely on physical properties or exogenous tracers, making it difficult to reveal the precise molecular makeup of tissues; (3) Potential radiation exposure during detection. CTA requires X-rays, while PET uses radioactive tracers, both of which can pose certain risks from ionizing radiation to patients.

However, these limitations call for alternative or complementary imaging approaches that can offer higher spatial

resolution, enhanced molecular specificity, and minimal safety concerns. One such technique is Raman spectroscopy, which has gained increasing attention for its capacity to address some drawbacks of conventional methods.

Raman is a detection technique offering high-resolution, marker-free, and radiation-free spectral analysis [24]. Because the typical incident light is visible or near-infrared, the theoretical limit resolution is about 200–500 nm [25–29]. Moreover, Raman technique usually employs spectrometers with high-density gratings, so it offers a much better spatial resolution and imaging quality than conventional methods [30, 31]. The Raman spectra of each substance are unique, which allows us to distinguish them without additional markers [32]. Meanwhile, in the process of obtaining Raman spectra, neither radiation source nor additional radiated electromagnetic waves are generated [33, 34]. Thus, Raman technology has a broad application prospect in biochemical detection.

This article reviews the progress of Raman and its derivatives in cardiovascular disease, especially in the field of atherosclerosis. Section "The principle and technical classification of Raman Spectroscopy" is dedicated to the principle of Raman spectroscopy and the technical classification of Raman spectroscopy. Section "Raman and other imaging techniques in CVD" introduces the applicability of Raman spectroscopy and its comparison with traditional methods (MRI, CTA, PET, FTIR, NIRF, OCT and IVUS) at different targets of diagnosing in atherosclerosis diagnosis. Section "Conclusion" illustrates the applicability of Raman spectroscopy in advanced cardiovascular diseases.

The principle and technical classification of Raman Spectroscopy

Raman spectroscopy provides valuable molecular information about diverse biological materials without requiring external labels or probes [35]. It is based on the inelastic scattering of light by molecules, which results in a frequency shift of the scattered light relative to the incident light. This frequency shift, which is called the Raman effect, reflects the vibrational modes of the molecules and can be used to identify and characterize them. The principle of Raman spectroscopy is illustrated in Fig. 1.When photons collide with matter, most of them undergo elastic scattering, and the frequency of the scattered light is identical to that of the incoming light, a phenomenon known as Rayleigh scattering [36]. The remaining fraction undergoes inelastic collisions, producing scattered light at frequencies different from those of the incoming light, which is called Raman scattering [37]. Raman scattering includes two types: (1) Stokes scattering. The sample molecules absorb photons to transition from the ground state to the excited state. Because the molecules in the excited state are unstable, they release photons and transition to vibrational state. Since the energy released by the deexcitation process is smaller than the energy from the ground state excitation to the excited state, the frequency and energy of the released photons are smaller than the incident photons [38]; (2)Anti-Stokes scattering. Molecules in the vibrational level absorb photons to transition to the excited virtual state, and similar to the stokes process, molecules in the excited virtual state are also unstable; they release photons and transition to the ground state. The energy released in this process is greater than the energy required to transition from the vibrational level to the excitation virtual state, so that the frequency and energy of the released photons are greater than those of the incident photons [39]. The typical electronic energy level diagram is shown in Fig. 1A. The Raman scattered light can be either lower or higher in frequency than the incident light, which corresponds to Stokes and anti-Stokes scattering, respectively [36]. The frequency difference between the incident and scattered light is called the Raman shift, which is proportional to the energy difference between the initial and final states of the molecule. By measuring the intensity and frequency of the Raman scattered light, one can obtain a spectrum that reveals the molecular vibrations of the sample. The Raman spectra comprise multiple bands, with their position depending on the vibrational frequency of each functional group in the sample molecules [40]. The intensity of Raman signal depends on the vibrational mode and the number and species of chemical bonds in the sample, so Raman spectrum has specificity for the detection of chemical structure.

However, Raman scattering is a very weak process, and the intensity of the Raman signal is often limited by the background noise and fluorescence from the sample or the optical components [36]. To overcome this limitation, several techniques have been developed to enhance the Raman signal by using nonlinear optical processes that involve multiple light beams interacting with the sample. These techniques are collectively called Coherent Raman spectroscopy (CRS). Another effective approach to overcome this limitation is Surface-Enhanced Raman Scattering (SERS). Recently, a novel technique known as Tip-enhanced Raman spectroscopy (TERS) has emerged, which integrates the capabilities of Scanning Probe Microscopy (SPM) with Raman spectroscopy, enabling chemical analysis at the nanoscale. By leveraging the lightning rod effect and localized surface plasmon resonance of a nanometer-sized tip, TERS significantly enhances the electromagnetic field near the tip, thereby greatly amplifying the Raman signal and obtaining Raman images with high spatial resolution and signal-to-noise ratio. However, the lengthy time required to obtain a single image limits the scope of its

Table 1 Summary of Raman related techniques

Raman related technology	Principle	Advantages	Reference
The traditional Raman	Photons inelastically scatter with matter, producing scattered light with frequencies different from the incident light	It is label-free, non-invasive, and can detect aqueous samples directly; It can provide molecular information of proteins, lipids, nucleic acids, and carbohydrates	[33, 63, 64]
Surface Enhanced Raman Scattering (SERS)	It uses enhanced nanostructures (mainly gold, silver, copper) to enhance the Raman scattering signal of the sample adsorbed on the surface	It is fast due to the unique ability to amplify the Raman signal up to 15 orders of magnitude; It can achieve single-molecule detection and high specificity; It can be combined with microfluidics and biosensors for multiplexed analysis	[65–67]
Stimulated Raman Spectroscopy (SRS)	When two beams whose frequency difference is the same as the molecular vibration frequency are irradiated on a matter, a dramatically enhanced SRS signal is generated	It's not affected by the non-resonant background; It can provide high sensitivity and specificity for label-free imaging of biological samples; It can be integrated with fluorescence microscopy for multimodal imaging	[62, 68]
Coherent Anti-Stokes Raman Spectroscopy (CARS)	Similar to SRS, but based on the principle that when pump light, Stokes light and probe light interact with molecules nonlinearly, with energy transfer, SRL and SRG signals are generated	It has high detectability, can penetrate deep into tissues, reduces photodamage, and can form three-dimensional images; It can provide chemical contrast and spatial resolution for label-free imaging of biological samples	[54, 69]
Tip-enhanced Raman Spectroscopy (TERS)	It enhances the Raman scattering signal by leveraging the lightning rod effect and localized surface plasmon resonance generated by nanometer-sized tips.	It is capable of surpassing the diffraction limit at the sub-micrometer scale, achieving nanoscale spatial resolution; It significantly enhances the Raman scattering signal, enabling single-molecule detection; and it is label-free.	[199, 200]

applications. Although Tip-Enhanced Raman Spectroscopy (TERS) has demonstrated superior analytical capabilities, its application in cardiovascular disease research has been sparsely reported. It is anticipated that in the future, TERS will be more extensively utilized in cardiovascular disease research, potentially offering novel tools and methodologies for diagnosis and treatment. At present, more than 25 types of Raman techniques have emerged [41], including Surface CRS, SERS, etc. In this paper, we place particular emphasis on Raman techniques that are commonly utilized in cardiovascular disease.

SERS is a technique that can greatly amplify the Raman signal of molecules that are adsorbed on or near metal nanostructures, such as silver, gold, or copper [42]. SERS can provide rich information about the molecular structure, composition, and interactions of the analytes, with high sensitivity and selectivity [43]. The principle of SERS is based on two main mechanisms: electromagnetic and chemical enhancement [44]. Both mechanisms rely on the interaction between the incident light and the metal nanostructures, which can generate Localized Surface Plasmon Resonances (LSPRs) [45]. LSPRs are collective oscillations of free electrons on the metal surface, which can produce strong local electric fields near the metal surface. These fields can enhance both the excitation and the scattering of the Raman signal of the nearby molecules. The electromagnetic enhancement is the dominant mechanism of SERS, which can account for up to 10^{10}-fold enhancement of the Raman signal. The electromagnetic enhancement depends on several factors, such as the shape, size, arrangement, composition, and dielectric environment of the metal nanostructures, as well as the wavelength, angle, and polarization of the incident light [46–48]. Generally, the electromagnetic enhancement is maximized when the LSPR frequency matches the incident light frequency. Moreover, when there are small gaps or sharp tips between adjacent metal nanostructures, the local electric fields can be further enhanced and localized, forming so-called "hot spots" that can provide higher SERS enhancement factors [49, 50]. The chemical enhancement is a minor mechanism of SERS, which can account for up to 103-fold enhancement of the Raman signal [51]. This mechanism occurs due to the charge transfer between the metal and the molecule, which modifies the molecular energy levels and polarizability. The chemical enhancement depends on several factors, such as the affinity, adsorption site, adsorption mode, and orientation of the molecule on the metal surface, as well as the relationship between the incident light and the charge transfer energy level [52]. Generally, the chemical enhancement is maximized when the incident light matches the charge transfer energy level.

Stimulated Raman Scattering (SRS) and Coherent Anti-Stokes Raman Scattering (CARS) are two major forms of CRS techniques, which have wide applications in various fields [53]. To excite and probe the vibrational modes of the sample, SRS and CARS use two laser beams with different frequencies, which are called the pump and the Stokes beams. The frequency difference between the pump and the Stokes beams must match a vibrational frequency of the sample for resonance to occur. The main difference between SRS and CARS is in the detection scheme and the signal generation mechanism.

In SRS, the pump and Stokes beams are modulated at a certain frequency, typically in the megahertz range. When

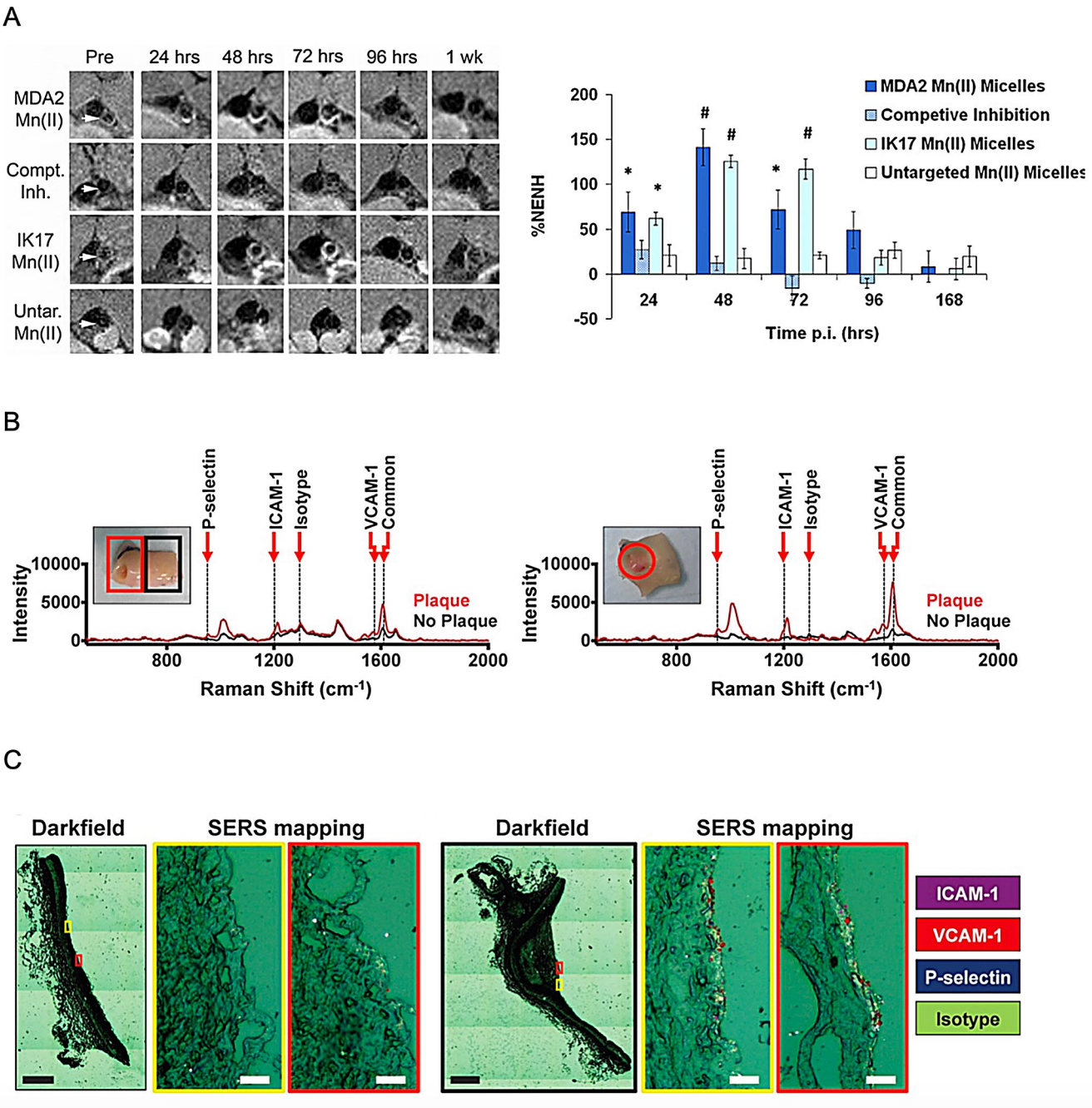

Fig. 2 MRI and SERS imaging. **A** MRI imaging of apoE-/- mice injected with Mn micelles. MRI image of abdominal aorta (white arrow) injected with Mn (0.05 mmol Mn/kg) micelles. Normalized Enhancement Percentage (%NENH) value represents the contrast to noise ratio before and after imaging. (Untar = untargeted; Compt. Inh. = competitive inhibition; MRI = magnetic resonance images; p.i. = post-injection; Pre = pre-injection.) From reference [79]. **B** A human coronary artery was isolated from the heart of a patient who underwent heart transplantation. Spectral analysis of atherosclerotic (red line) and non-atherosclerotic (black line) areas of intact (left penal) and open (right penal) arteries was performed by SERS. From reference [84]. **C** SERS mapping was then performed against ICAM-1 (purple), anti-VCAM-1 (red), anti-P-selectin (blue), and isotype (green) BFNPs. The yellow and red boxes in each dark field image correspond to the yellow and red boxes in the right SERS image. Scale bars: 500 μm (black bar) and 20 μm (white bar). From reference [84]

they are both focused on the sample, they induce a stimulated Raman process that transfers energy from the pump beam to the Stokes beam if resonance occurs [54]. This results in a decrease in the intensity of the pump beam (called stimulated Raman loss, or SRL) and an increase in the intensity of the Stokes beam (called stimulated Raman gain, or SRG) [55]. By using a lock-in amplifier or a balanced detector, one can measure the SRL or SRG signals

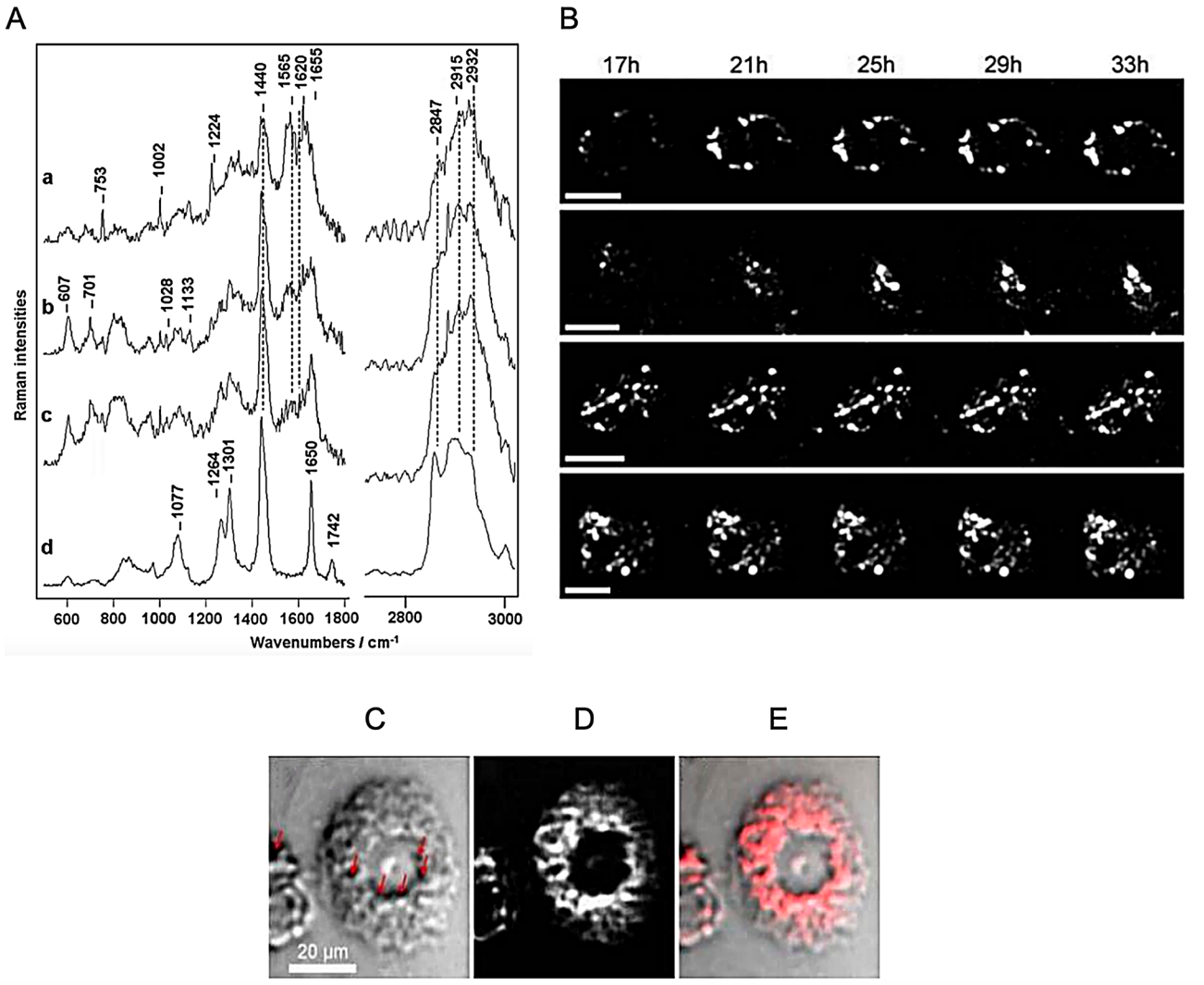

Fig. 3 CARS and SRS imaging. **A** CARS imaging of cellular lipid droplets in macrophages treated with miRNA-33 and treated with acetylated low-density lipoprotein (acLDL) for 24 h (miRNA-33 mimic) and control groups (ctrl mimic). Right panel is voxel wise quantitative lipid droplet volume analysis. Scale bar = 10 μm. From reference [106]. **B** Raman probes were introduced into living rabbits to obtain spectral signals at different locations. (a) distal aorta, (b) thoracic aorta, (c) aortic arch, (d) ascending aorta. From reference [106]. **C** CARS signal **D** SRS signal **E** mixed signal (SRS signal is red, CARS signal is gray). SRS imaging of human macrophages at 2125 cm^{-1} after incubation in d_{31}-palmitic for 24 h. From reference [110]

as a function of the frequency difference between the pump and Stokes beams, and obtain the vibrational spectrum of the sample. The advantage of SRS is that it does not produce any background signal from non-resonant processes or fluorescence, and it has a linear dependence on the concentration of the sample [56]. The disadvantage of SRS is that it requires sensitive detection systems and modulation techniques to measure small changes in intensity.

In CARS, the pump and Stokes beams are not modulated, but rather combined with a third beam, called the probe beam, which has the same frequency as the pump beam [57–60]. When they are all focused on the sample, they generate a new beam at a higher frequency, called the anti-Stokes beam, through a four-wave mixing process [61]. The frequency of the anti-Stokes beam is given by ωAS = 2ωP - ωS, where ωP, ωS, and ωAS are the angular frequencies of the pump, the Stokes, and the anti-Stokes beams, respectively. The intensity of the anti-Stokes beam is proportional to the square of the number of molecules that are resonant with the frequency difference between the pump and the Stokes beams. By measuring the anti-Stokes signal as a function of the frequency difference between the pump and the Stokes beams, one can obtain the vibrational spectrum of the sample. The advantage of CARS is that it produces a strong signal that can be detected easily and allows for fast imaging. The disadvantage of CARS is that it also produces

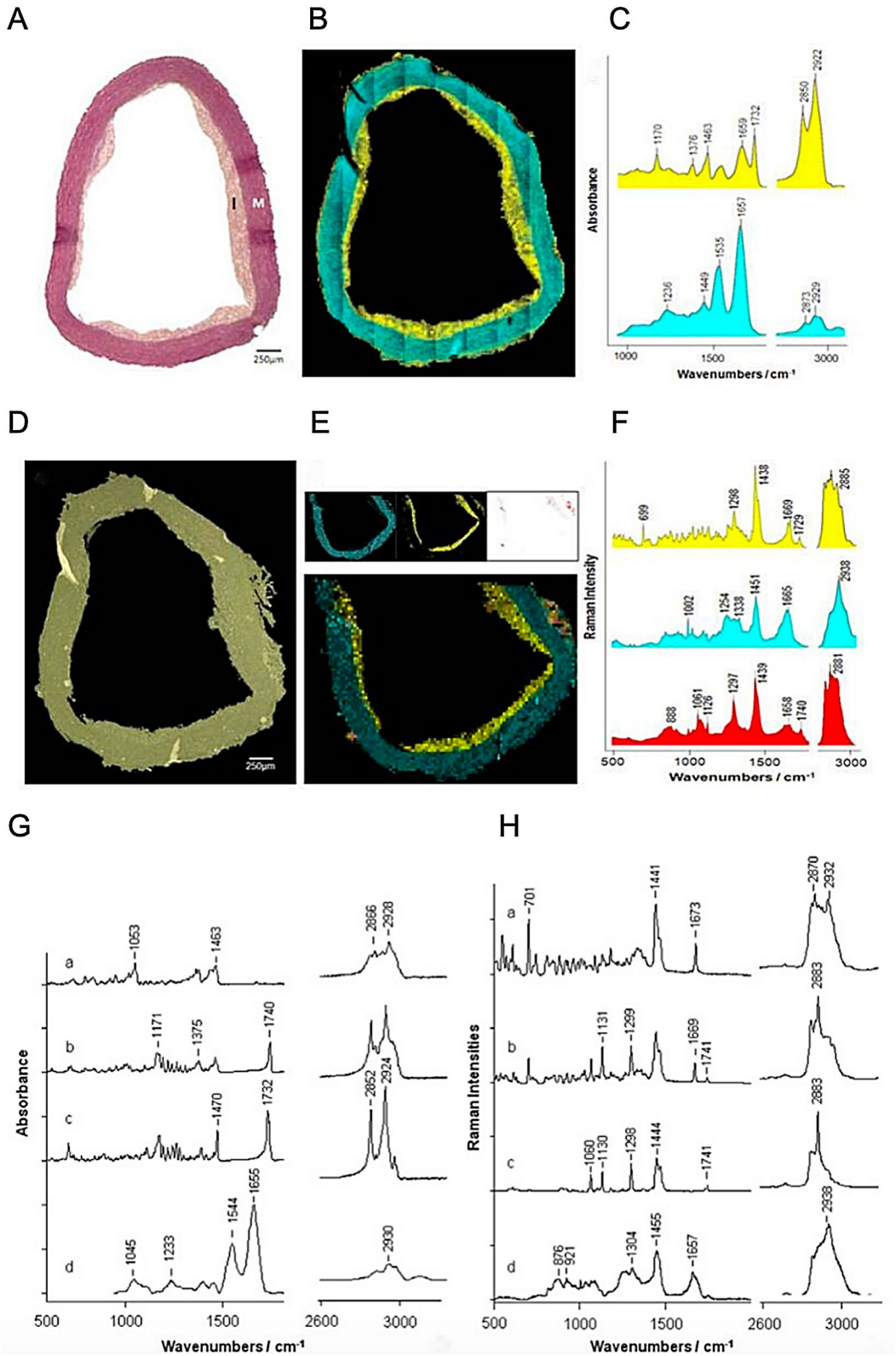

Fig. 4 FTIR and Raman imaging. **(A)** Cross section of thoracic aorta stained with EVG (normal media (M)) FTIR **(B)** and Raman **(E)** show the unstained cross-section of the thoracic aorta **(D)** reconstructed with the vac algorithm. **(C)** and **(F)** are the infrared and Raman spectra of this cross section. From reference [121]. **G** and **H** are the reference infrared and Raman spectra of typical atherosclerotic plaque. Cholesterol (a), cholesterol esters (b), triglycerides (c), and collagen (d). From reference [121]

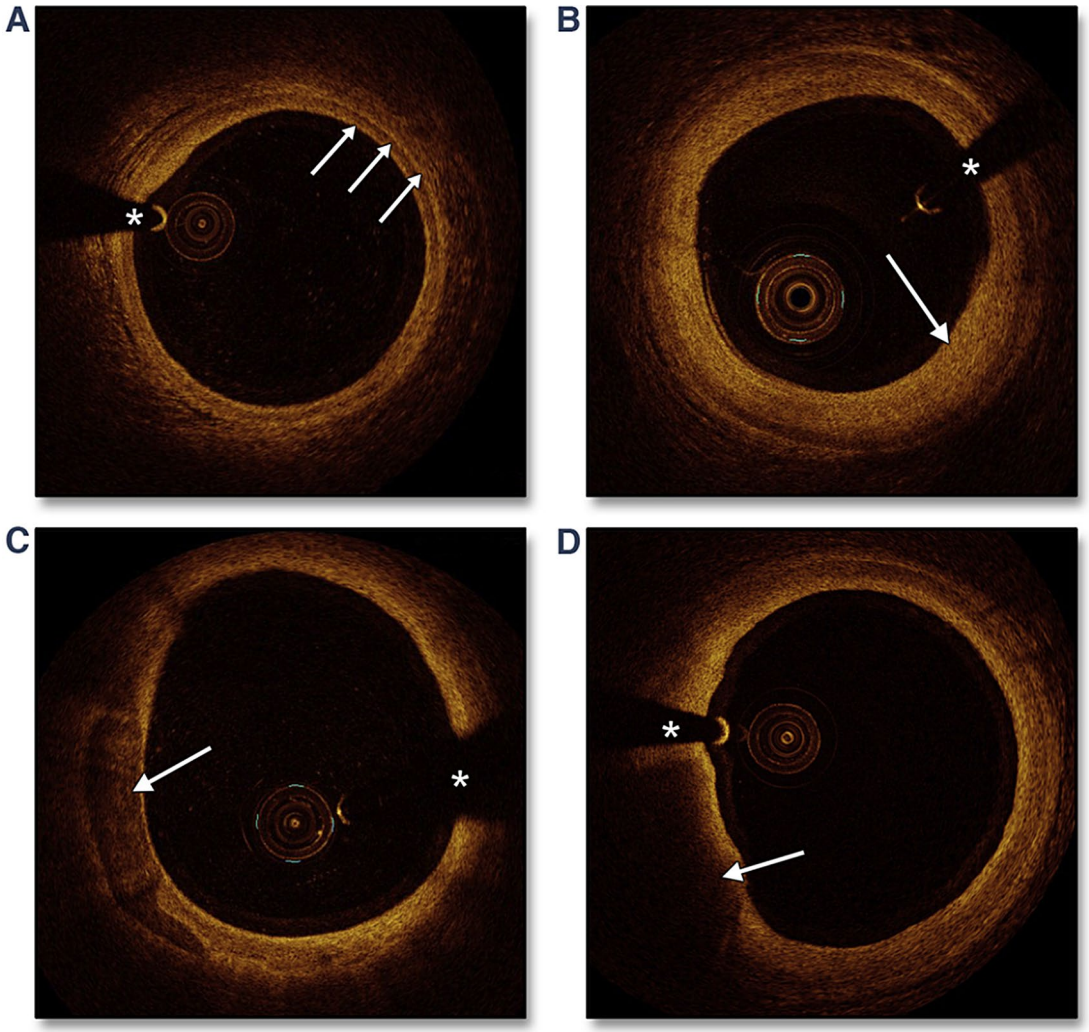

Fig. 5 Imaging of OCT. **(A)** Composition of the normal coronary artery, with white arrows depicting the internal elastic lamina, media and external elastic lamina. **(B)** Concentric fibrous plaque. **(C)** Calcified plaque. **(D)** Necrotic core. *Guidewire artifact. From reference [141]

a background signal from non-resonant processes that can interfere with the resonant signal and reduce the contrast and the chemical specificity [62]. We summarize the advantages of all the above Raman techniques in Table 1.

Raman and other imaging techniques in CVD

There are a series of imaging techniques, including MRI, PET, CTA, IVUS, OCT, etc., which can be used in researches of CVD [70]. We indicate the benefits of Raman, a potential cardiovascular-related imaging technique, by comparing it to conventional imaging methods. Moreover, we outline a classification of target detection into four distinct categories based on the different types of targets identified in various studies using different imaging techniques. These categories include marker-based target, cellular target, tissue-specific target, and vascular target.

Biomarker-based target detection in atherosclerosis

One of the most widely used techniques in CVD research is MRI, which can provide images of the arterial wall and plaque morphology [71, 72]. Hartley A, Haskard D, et al. indicated oxidation-specific epitopes (OSEs) that are present in oxidized low-density lipoprotein (oxLDL) and LDL-derived oxidized phospholipids [73]. These OSEs, which have been considered to be related to CVD in a 15-year-study, can be recognized by C-reactive protein, complement system proteins and IgM antibodies [74, 75]. Various molecular probes have been developed to bind OSEs. MRI monitors disease progression by detecting the combination of OSE and molecular probes. For example, the human-derived Fv antibody, IK17, is a fragment with high specificity for OSEs on oxLDL, whereas the murine monoclonal IgG MDA2 antibody is specific for malondialdehyde-lysine, which is an OSE on oxLDL. They can bind to micelles

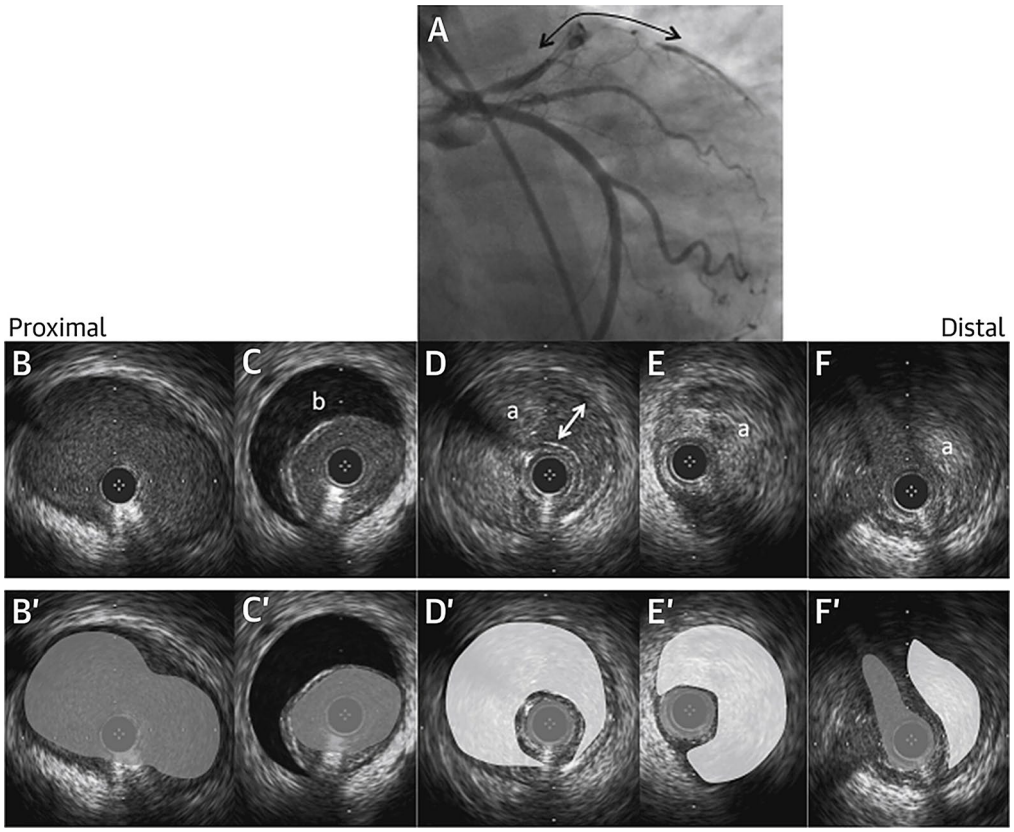

Fig. 6 Imaging of IVUS. **(A)** Coronary angiography showed a severe stenosis from proximal to distal left anterior descending artery (double-headed black arrow). Corresponding intravascular ultrasound imaging (B to F, with duplicated and annotated images B' to F') showed a spontaneous dissection (double-headed white arrow), intramural hematoma **(a)** and contrast retention **(b)**. The gray areas on the annotated frames (B' to F') indicated the true lumen, the white areas indicated the false lumen, and the black area indicated contrast retention. The nondissected image slice **(B)** showed a nonatherosclerotic coronary artery that was typical for spontaneous coronary artery dissection. From reference [149]

formed by the combination of gadolinium and manganese, which are both considered excellent contrast agents for MRI, to form targeted probes. These probes can then bind to OSEs, allowing for the in vivo monitoring of atherosclerotic progression [76–79], as shown in Fig. 2A. However, MRI has some inherent limitations due to its technical nature, such as long imaging time and low sensitivity [80, 81]. To address the major weakness of MRI, ultrasmall paramagnetic iron oxide particles (USPIOs; 10–50 nm in diameter) have been developed to detect atherosclerotic diseases [82]. However, the utilization USPIOs presents several limitations. Firstly, the inherent toxicity of USPIOs poses potential risks. Secondly, the method lacks a quantitative analysis capability, making it challenging to accurately measure the size and severity of atherosclerotic plaques. Moreover, the study using USPIOs did not conduct long-term monitoring, leaving the long-term effects of USPIOs undetermined. Additionally, the low-resolution issue inherent to MRI was not addressed, which could limit the detailed visualization of atherosclerotic plaques [83]. Due to the two main limitations of biomarkers, including the toxic side effect and type, a few researches are reported in atherosclerosis clinical diagnosis.

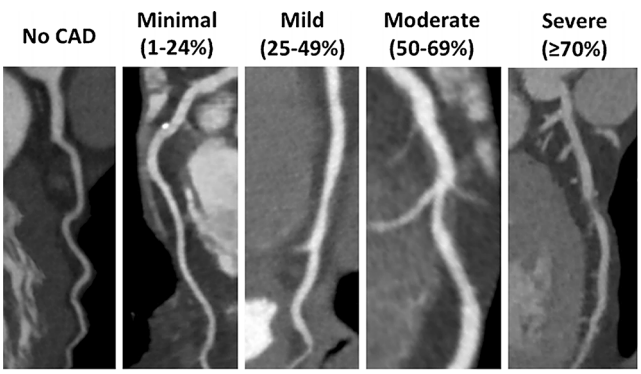

Fig. 7 CTA diagnoses the degree of CAD blocking. From reference [156]

Due to the limitations of these MRI technique, Raman can be a promising alternative/ better alternative. SERS, which has been reported to be used to detect atherosclerosis at the biomarker level, employs metals such as gold, silver and copper to enhance the Raman signals of target

Table 2 Summary of the imaging detection for atherosclerosi

Technique	Resolution	Principle	Purpose	Limitation	Raman's advantages	Reference
MRI	0.1–1 mm	Signals generated by hydrogen nuclei in a magnetic field, processed by computer reconstruction, and imaged	Plaque location, degree of vascular stenosis, morphology, composition, inflammation, and neovascularization	Long imaging time; Poor sensitivity and specificity; No real-time detection; Label-dependent	Short imaging time; high sensitivity in detecting specific biomarkers; being able to achieve real-time detection combined with catheters; label-free (SERS)	[71, 72, 80, 81, 153, 196, 197]
PET-CT	1–10 mm	Isotope-labeled drugs (imaging agents) with positron emission are injected into human bodies and detected by varying attenuation rates in different tissues	Plaque metabolism, calcified sites, inflammation, vulnerability, and prediction of future cardiovascular events	Dependent on radioactive substances and susceptible to interference from blood signals; Limited spatial resolution; High cost and radiation exposure	Non-radioactive; immunity to interference; no significant artifacts; high spatial resolution (CRS)	[85, 86, 97–100]
FTIR	10 μm	Infrared radiation acts on matter and measures the frequency of molecular vibration. Substances are then detected by infrared spectroscopy	Plaque chemical composition distribution and identification of lipid-rich necrotic core, calcification, collagen, and elastin	Low spatial resolution and long wavelength cause energy loss; Sensitive to water and atmospheric interference; Limited penetration depth;	High spatial resolution; SRS being able achieve high contrast without significant interference by non-resonant background; CARS being able to penetrate deep into tissues (SRS、CARS)	[114, 122, 123, 198]
NIRF	1 μm	A specific near-infrared fluorescence probe is irradiated with a laser source and the photon signal stimulated by the probe is collected to convert the image	Plaque inflammation, location, and vulnerability	Developer is toxic, photobleached; Low resolution; Limited penetration depth;	High resolution (CARS)	[132, 133, 137]
OCT	10 μm	The beam is projected onto the tissue or specimen being imaged and reflected by the microstructures at different distances	Stenosis degree, plaque shape, plaque location, and plaque composition	Sensitive to motion artifacts, stabilization or synchronization equipment may be required; Highly sensitive to scattering and absorption; Limited field of view; Invasive procedure	Non-invasive (CARS)	[145, 146, 153]
IVUS	100 μm	Ultrasound imaging using a catheter combined with an ultrasound probe that receives the reflected echo	Stenosis degree, plaque shape, plaque location, and plaque burden	Low resolution and contrast of soft tissue and plaque components; Limited field of view; High operator dependence and variability; Invasive procedure	High resolution; high contrast; non-invasive (CARS)	[147, 150–154]
CTA	0.5–1 mm	In vivo contrast imaging of developer by CT	Stenosis degree, plaque location, size, calcification, and luminal morphology	Limited time resolution; Exposure of patients to ionizing radiation; May cause allergic reactions, nephrotoxicity, or exudation	Short imaging time offering possiblity of high time resolution; non-radioactive;	[157–161]

molecules by a factor of 10^6 [42]. Therefore, SERS can enable the detection of biomarkers in CVD at low concentrations and with high specificity. Atherosclerosis involves some biomarkers such as intercellular adhesion molecule 1 (ICAM-1), vascular cell adhesion molecule 1 (VCAM-1), and P-selectin, which can be detected by SERS [84]. They are expressed by endothelial cells, smooth muscle cells, and macrophages respectively. These cells are related to CVD. In order to detect these biomarkers more accurately, Jonathan N., Steven M., et al. designed an antibody-functionalized gold nanoprobe (BFNP) composed of citrate-reduced gold nanoparticles, Raman reporter molecules, polyethylene glycol (PEG), and specific antibodies [84]. Figure 2B shows the SERS images of different coronary arteries injected with

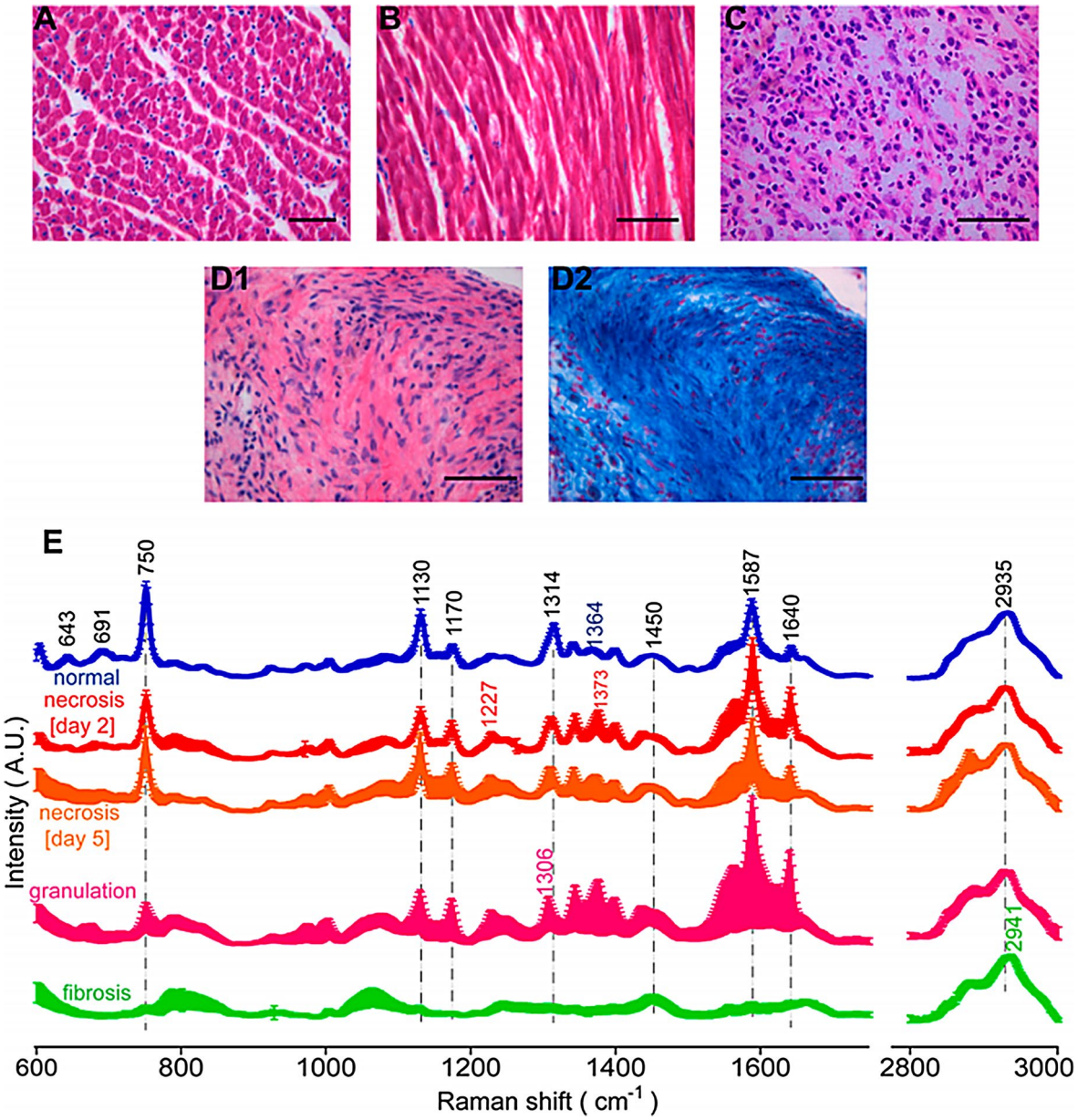

Fig. 8 Histological examination and Raman spectra derived from cardiac tissues. **(A)** H&E-stained specimen of normal heart. **(B−D)** H&Estained specimens of myocardial infarction obtained at various postligation time points: day 2 **(B)**, day 5 **(C)**, and day 21 **(D1)**. **(D2)** Azan staining of myocardial infarction at day 21. Histology shows coagulation necrosis **(B)**, granulation tissue **(C)**, and fibrotic scar **(D1 and D2)**. **(E)** Raman spectra (means ± one standard deviation) of normal tissue [$n=2$; number of spectra (NOS) = 150], necrotic tissue on day 2 ($n=3$; NOS = 150), necrotic tissue on day 5 ($n=4$; NOS = 150), granulation tissue on day 5 ($n=4$; NOS = 500), and fibrotic tissue on day 21 ($n=2$; NOS = 150). The scale bars are 50 μm.
Reprinted with permission from reference [183]

anti ICAM-1, anti VCAM-1 and anti P-selectin. The Raman spectra of these arteries revealed the presence of the biomarkers in the plaque region. The high positivity of ICAM-1, VCAM-1, and P-selectin in atherosclerotic endothelial cells was confirmed by SERS microscopy of atherosclerotic and nonatherosclerotic tissue areas (Fig. 2C). Moreover, the darkfield contrast of BFNP at the endothelial surface of atherosclerotic tissue was markedly higher than that of nonatherosclerotic regions, indicating a higher density of BFNP at this site. These results show the advantages of SERS, containing high specificity, high sensitivity, rapid imaging time, and no photobleaching. These advantages make SERS have the potential to become a powerful tool for CVD detection.

Cellular target detection in atherosclerosis

PET is an imaging modality that employs radioactive substances, such as positron-emitting isotopes and

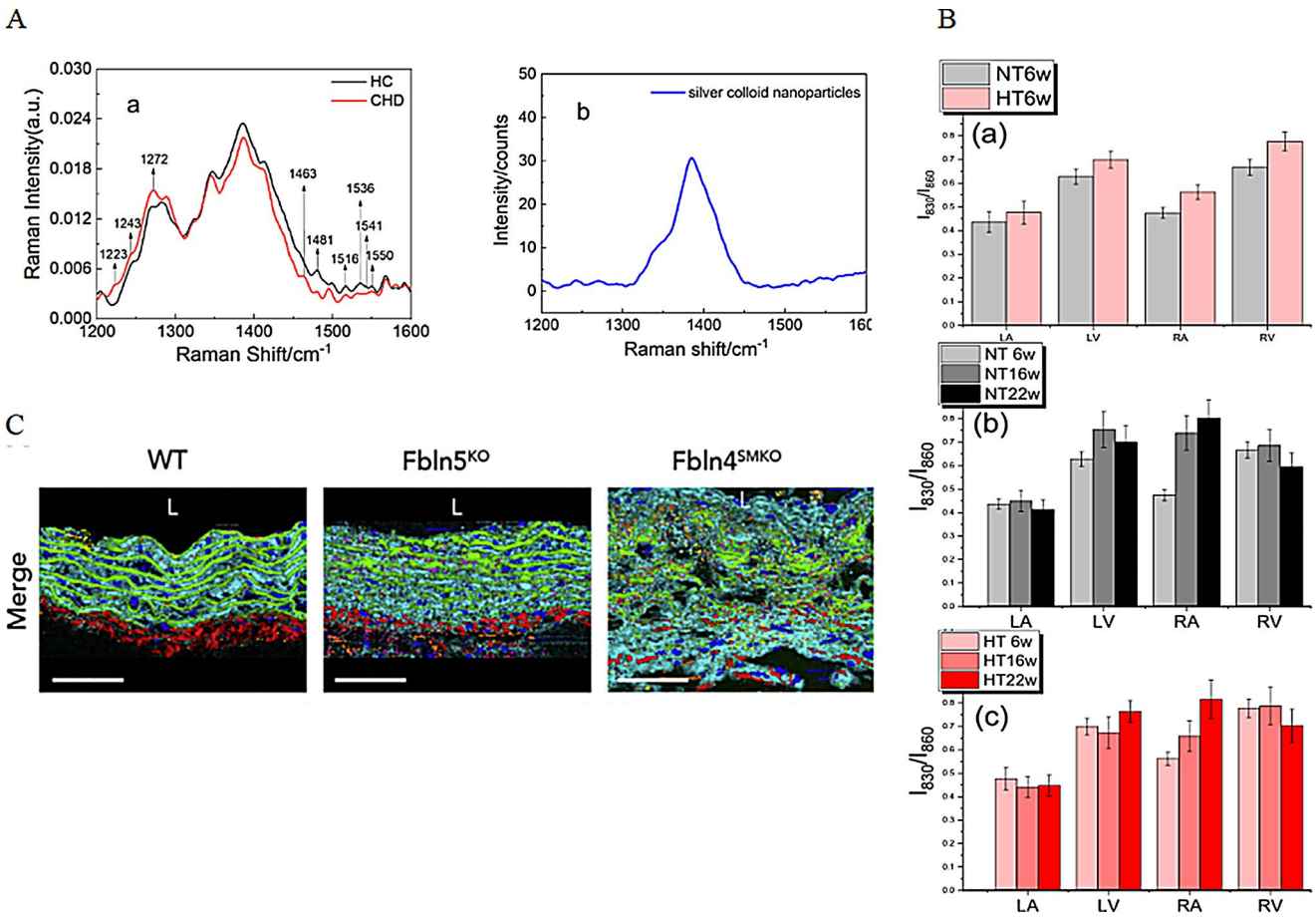

Fig. 9 Raman imaging in other cardiovascular diseases. **A**(a) Urine SERS spectra of CHD and healthy controls (HC) SERS spectra (b) SERS spectra of Raman substrate silver colloids. The intensity of nine Raman peaks (1223 / 1243 / 1272 / 1463 / 1481 / 1516 / 1536 / 1541 / 1550 cm^{-1}) in the average SERS spectra of CHD and HC were found to be different. From reference [168]. **B** Raman spectra at 830 / 860 cm^{-1} intensity ratio (i830 / i860). NT indicates normotensive Dahl/SS rat; HT, hypertensive Dahl/SS rat; LV, left ventricle; RV, right ventricle; LA, left atrium; and RA, right atrium. From reference [185]. **C** Fbln4SMKO: the SMC-specific Fbln4 knockout mice, which will develop thoracic aortic aneurysms. Fbln5KO: the Fbln5 knockout mice, which only develop aortic elongation and tortuosity. Image colors include fibers (green), collagen fibers (red), nuclei (blue), aggrecan (yellow), versican (pink), lipids (orange), and residual ECM (cyan). From reference [189]

isotope-labeled radiotracers, to quantify the attenuation rates of varying tissue densities [85, 86]. PET has several imaging agents for atherosclerosis, including ^{18}F-fluorodeoxyglucose (^{18}F-FDG), ^{18}F-sodium fluoride (^{18}F-NaF), ^{68}Ga-DOTATATE, and ^{68}Ga-PENTAXIFOR [87, 88]. ^{18}F-FDG is preferentially taken up by macrophages in high-risk plaques in response to inflammation [89–91]. This suggests that 18F-FDG may have substantial utility in the identification of high-risk atherosclerotic plaques. ^{18}F-NaF serves as a bone-seeking tracer, marking areas of plaque calcification. This can act as an early indicator of atherosclerosis, a stage characterized by the dedifferentiation of smooth muscle cells leading to intimal calcification [89, 92]. ^{68}Ga-DOTATATE is employed for the detection of macrophages through its binding to the somatostatin subtype-2 receptor (SSTR2) [93]. A study conducted by Tarkin JM et al. has identified the specific expression of the SSTR2 gene in atherosclerotic inflammation [94]. ^{68}Ga-PENTAXIFER has a high affinity for the C-X-C Motif Chemokine Receptor 4 (CXCR4), which is expressed in both macrophages and smooth muscle cells [95]. Concurrently, a study by Weiberg D, Thackeray JT et al. has demonstrated an association between ^{68}Ga-PENTAXIFER and cardiovascular [96]. During imaging, the visualization produced by the interaction between target cells and imaging agents is affected by signals from neighboring tissues. This, along with the inherent limitations of PET's spatial resolution capabilities, can result in images with low spatial resolution (≈5 mm) [97, 98]. Furthermore, imaging agents requires sufficient time to accumulate at the site of interest, which may not align with the clinical needs of patients requiring rapid testing [99]. While PET imaging enables visualization of plaque metabolic processes, it also presents certain drawbacks. These include reliance on the accumulation of radioactive materials that may potentially

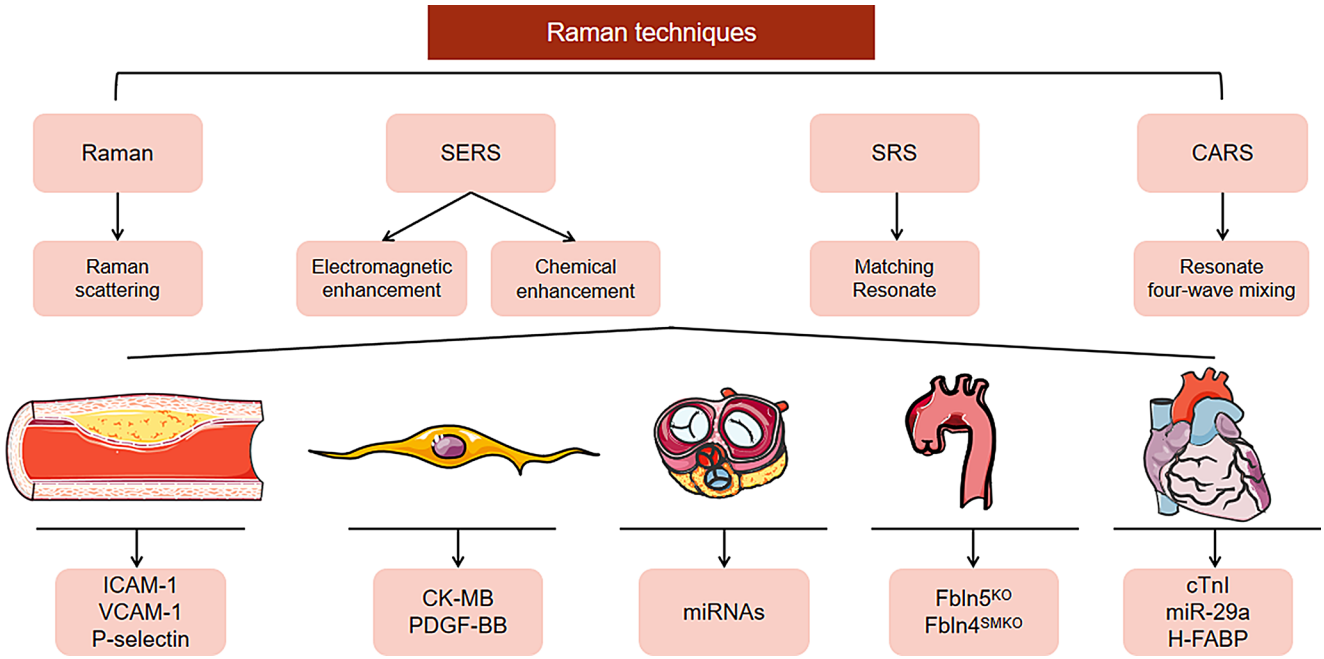

Fig. 10 Raman is currently the main application in cardiovascular disease. Artwork is provided by SERVIER

harm the body, signal interference from adjacent tissues (particularly blood) and high cost and complexity [100].

In contrast to the aforementioned limitations, CRS (include CARS and SRS), a derivative of Raman technology, circumvents these drawbacks and offers advantages such as high resolution, high specificity, and the ability to provide almost real-time imaging. CARS can detect atherosclerosis at subcellular structures by tuning the pump and Stokes frequencies to resonant with the symmetrical CH_2 vibration, which exhibits high sensitivity and selectivity to lipid droplets and lipid membranes [101, 102]. In their seminal work, Mireille O, Hasini E, et al. employed CARS to elucidate the role of microRNA-33 (miRNA-33) in lipid droplet accumulation within macrophages and its subsequent impact on apoptotic cell clearance via an autophagy-dependent pathway, which has been linked to pro-atherosclerotic processes [103–105]. The researchers adeptly utilized CARS to demonstrate an increase in lipid accumulation within macrophages following treatment with miRNA-33. A subsequent investigation probed the chemical composition of atherosclerotic plaque in rabbits, leveraging the detection of Raman spectral signals via CARS in conjunction with molecular probes [106]. The study observed the manifestation of fatty C-H bond stretching within the 2847–2915 cm^{-1} region, as illustrated in Fig. 3A. Normal tissue was imaged in resonance with the peak of the C-H stretching vibration at 2930 cm^{-1}. These experiments underscore the advantages of CARS in its immunity to interference from blood and other tissue signals.

While both SRS and CARS offer unique advantages, a key strength of SRS lies in its immunity to any background signals arising from non-resonant processes or fluorescence [107, 108]. This characteristic enhances the specificity of SRS, enabling it to more accurately detect and distinguish different chemical components within a sample. Additionally, this immunity to background signals allows SRS to generate clearer images with less noise compared to CARS [109]. Furthermore, both SRS and CARS share the advantage of rapid imaging, which is particularly beneficial for clinical needs requiring quick results. In their research, Lara S, Tobias M, et al. utilized SRS to investigate the concentration and heterogeneity of lipids within atherosclerotic plaque and between cells [110]. The team used the intensity of the scattering peak at 2125 cm^{-1} in the Raman spectrum to monitor the uptake of the d31-palmitic acid, a deuterated lipid trace, by cells, and subsequently generated CARS, SRS, and composite images of the same macrophage undergoing d_{31}-palmitic acid uptake (Fig. 3B, C, D). It was observed that the nonresonant background in the CARS image, primarily influenced by the water environment, diminished the contrast between lipids and surrounding media. In comparison, SRS imaging exhibited superior contrast without significant interference artifacts (as indicated by the red arrow in Fig. 3B. Figure 3E presents the SRS signals of four living macrophages at different time points [110]. Notably, an enhancement in the SRS signal was observed along with a change in location within macrophages in the first and second rows. This suggests that macrophages undergo morphological changes during incubation. The rapid imaging

capability of SRS and its absence of artifacts due to lipid heterotopia enabled the detection of this phenomenon. In contrast to other in vivo cell detection techniques that don't measure the same cell repeatedly, SRS demonstrated in this experiment the ability to track cellular metabolic processes. Additionally, due to the SRS wavelength being longer than CARS and traditional Raman, it has less phototoxicity and improves the penetration depth applied in tissues [111, 112]. Therefore, SRS is more suitable for living cell imaging than CARS, which is affected by a nonresonance background in water, as seen in Fig. 3B, C. The storage of lipid droplets was studied by using hyperspectral SRS imaging, demonstrating that Raman technology has the potential to become a new method for detecting atherosclerosis [113].

Tissue-specific target detection in atherosclerosis

FTIR achieves this by analyzing the interaction between matter and infrared radiation to detect molecular vibration frequencies [114]. FTIR spectroscopy, in conjunction with conventional optical microscopy, serves as an effective method for the histopathological analysis and detection of biochemical changes in atherosclerotic plaque [115–121]. In a study conducted by Annika L. et al., both FTIR and traditional Raman spectroscopy were utilized to investigate atherosclerosis in rabbits [121]. Figure 4A shows a cross-section of the thoracic aorta stained with EVG, highlighting the hyperplastic thickened intima, and normal media. Panels (D) depict the unstained cross-section of the thoracic aorta, with panel FTIR (B) and Raman (E) showing the same cross-section reconstructed with the vac algorithm. The spectra for FTIR and Raman are visible in panels (C) and (F), respectively. Referring to panels 4G and 4 H, lipid precipitation was detected on the intima, indicating the presence of cholesterol, cholesterol esters, and triglycerides. Furthermore, the distribution of cholesterol was observed within smooth muscle cells. The spectral distribution of lipids is also demonstrated in Fig. 4F. Though FTIR spectroscopy is a powerful analytical tool, it is inherently limited by its relatively low spatial resolution, which can impede the accurate acquisition of detailed information about a substance [122, 123]. Moreover, the extensive sample preparation required for FTIR can pose significant challenges for certain experimental setups. Unlike FTIR, Raman spectroscopy can analyze samples in their native state, including solids, liquids, and gases, without the need for complex preparation steps. With its superior spatial resolution, Raman spectroscopy is capable of revealing detailed information about molecular vibrations, thereby elucidating the characteristic biochemical components within tissues. This allows for a more detailed analysis and potentially more accurate diagnosis in the context of atherosclerosis.

CARS imaging presents an label-free approach to visualize plaque components, encompassing collagen, extravascular lipid precipitation, oxidized LDL aggregates, and lipid cells [124]. Groundbreaking research by Hanwei W, Ingeborg M et al. has demonstrated that CARS can discern the biochemical alterations of atherosclerotic plaque across various pathological stages [125]. This research employed label-free multimodal nonlinear optical microscopy, combined with sum-frequency generation (SFG) and CARS techniques, to visualize and quantitatively analyze lipids and collagen at high resolution, thereby effectively detecting different stages of atherosclerosis development. This provides a completely new approach for using optical techniques to quantitatively analyze atherosclerosis. Moreover, CARS does not necessitate photon electron resonance and can employ a longer excitation wavelength to reduce tissue scattering and increase the optical penetration depth, thereby mitigating photo-damage induced by multiphoton absorption [126]. However, due to the high sensitivity of CARS being achieved by limiting the spectral range, the ability of CARS to obtain comprehensive spectral information is restricted. Additionally, the weak Raman signals require longer acquisition times and stronger excitation, which may introduce potential issues such as photodamage. Coupling CARS with other techniques, for example, CARS endoscopy eradicates photobleaching to minimize interference from extraneous signals [127, 128]. This makes CARS effectively circumvent the artifacts caused by staining.

Vascular target detection in atherosclerosis

NIRF, OCT, IVUS, and CTA are the imaging methods that have demonstrated efficacy in the detection and characterization of plaque attributes [129–131]. NIRF is a technique that generates an image by irradiating a near-infrared fluorescent probe with a laser source within a specific spectral range and then capturing the excitation photon signal from the probe [132, 133]. This technique can be used for detecting proteases S, K, B, L and F expressed by macrophages and smooth muscle cells in atherosclerosis [134–136]. Cathepsins B, L, S, K, and V are important members of the cysteine protease family, widely present within macrophages in atherosclerotic plaques. These enzymes are primarily located in lysosomes and participate in the remodeling of the arterial wall through their elastase and collagenase activities. Specifically, Cathepsins B, L, and S are capable of degrading elastin and collagen, promoting plaque instability and rupture, thereby increasing the risk of cardiovascular events. Additionally, Cathepsins K and V, under the action of matrix metalloproteinases, further exacerbate the degradation of the extracellular matrix, facilitating plaque erosion and vascular wall remodeling. To enable real-time

intravascular detection of inflammation in atherosclerosis, Jaffer FA et al. developed a catheter-based NIRF imaging technique in 2008 [137], but the catheter lacked the ability to rotate and pull back, which limited the clinical application of this technology. They resolved this problem in 2011 and applied the technique to monitor arterial inflammation and stent healing in vivo [138]. However, single NIRF technology has limited clinical application. Therefore, it is often combined with OCT to provide high-quality coronary atherosclerosis imaging [139]. OCT is an intravascular imaging modality that produces cross-sectional vascular images using near-infrared light. It can provide accurate descriptions of plaque morphology, such as calcified plaque, calcified plaque, necrotic core, as shown in Fig. 5 [140, 141]. And it allows people to accurately measure the diameter of blood vessels and the length of lesions, which is helpful for percutaneous coronary intervention (PCI) treatment [142–144]. Additionally, OCT is useful for identifying thin capped fibroatheromas (TCFAs), but sometimes confounds angiographic abnormalities, making it difficult to identify lesions [145, 146]. IVUS is an intravascular ultrasound imaging modality used to detect vascular walls and atherosclerotic plaque [147]. It is usually compared with OCT, which is necessary to utilize contrast agents for blood clearance in the retraction process, as the optical signal would be attenuated by red blood cells [148]. The catheter for IVUS is combined with a micro-transducer and emits ultrasound as it passes through the blood vessel, receiving ultrasound reflection and converting it into a cross-sectional image, as shown in Fig. 6 [149]. However, IVUS detection has some disadvantages, such as manual correction of lumen area calculations, acoustic shadow of calcified tissue, difficulty in identifying vulnerable plaque and thrombus, among others [150–154]. CTA is a three-dimensional visualization of the vascular system after intravenous injection of an iodine-containing contrast agent and computer-processed images, as shown in Fig. 7 [155–158]. However, CTA does not detect early atherosclerotic lesions well due to vascular remodeling [159, 160]. Additionally, CTA detection relies on the contrast between the lesion site and surrounding normal vessels, making it unsuitable for detecting diffuse vascular disease (lesions occur in most arteries) [161].

Although these techniques (CTA、IVUS and OCT) offer many advantages in detecting the location and size of plaque in clinical settings, they also have drawbacks, such as an inability to identify the specific chemical composition of the plaque and their susceptibility to interference from other biological signals [129, 162]. However, the unique nature of the Raman spectra for each substance ensures that the Raman technique is less susceptible to interference from other impurity signals. Besides, the combination of Raman spectroscopy and fiber-based probes has the potential to reveal the chemical composition of intraplaque arteries in humans clinically [163, 164]. And Raman spectroscopy has been successfully applied to characterize the chemical composition of atherosclerotic plaque in sheep and human arteries in vivo in 2001 and 2006 [117, 165, 166]. Moreover, the technique of combining CARS with a catheter has enabled the real-time detection and spectral analysis of vascular plaque in rabbits. It demonstrates the feasibility of integrating Raman spectroscopy with catheter technology for clinical diagnosis [121, 167]. We summarize the previous methods for detecting atherosclerosis in Table 2.

Raman in advanced cardiovascular diseases

Raman spectroscopy has also made significant contributions to the diagnostic research of other advanced CVDs, such as coronary heart disease, rheumatic heart disease, and aortic aneurysm. For the detection of coronary heart disease (CHD), SERS has been used to discriminate urine samples from CHD patients and healthy individuals by finding significant differences in their Raman spectra (Fig. 7A) [168]. Moreover, Huinan Y, Chang Z et al., who proposed using SERS to diagnose CHD and determine the feasibility of PCI based on urine spectra of CHD patients, also suggested that platelet-derived growth factor-BB (PDGF-BB) may be associated with cardiovascular congestion in CHD patients [169]. SERS can detect the increased levels of the short noncoding RNA molecule miRNA-29a that have been associated with the development of a variety of CVDs, including vascular inflammation, myocardial infarction, and heart failure [170, 171]. Moreover, SERS can measure the ratio of phenylalanine and tyrosine as an indicator of inflammation in myocardial infarction [172]. As myocardial infarction progresses, blood monocyte levels increase and accumulate at thrombotic inflammatory plaque lesions, triggering the inflammatory processes, and resulting in a concomitant decrease in 5,6,7,8 - tetrahydrobiopterin (BH4), leading to reduced conversion of phenylalanine to tyrosine [173].These studies demostrate the high specificity and sensitivity of SERS in detecting cardiac enzymes in both whole blood and plasma samples, underscoring its potential applications in clinical diagnostics as a promising tool for the early diagnosis of myocardial infarction [174]. Furthermore, SERS can detect cardiac troponin I (cTnI) and heart-type fatty acid-binding protein (H-FABP) and improve the accuracy for early diagnosis of myocardial infarction [175]. Cunming H, Li M, et al., who utilized Raman reporters, 4-MP (1073.5 cm^{-1}) and XP013 (1377.3 cm^{-1}), to determine marker concentrations and achieved high sensitivity in detecting cTnl and H-FABP, showed that cTnI has high specificity for myocardial injury, but poor sensitivity in the early stage of myocardial ischemia and is not suitable for the early diagnosis

[176]. In contrast, H-FABP that can be rapidly released into the blood during early myocardial injury and has a better correlation with the area of myocardial injury is a better biomarker [177–179]. Creatine kinase-MB (CK-MB) is also sensitive for acute myocardial infarction (AMI) diagnosis and can be tested with cTnI to detect AMI with early diagnostic accuracy [180]. Hyangah C, Sangyeop L, et al. used a SERS-based competitive immunoassay to detect these two cardiac markers, demonstrating its potential for early AMI diagnosis [174]. Raman spectroscopy was also used to compare normal myocardial cells with cells in the myocardial infarction area, and Nanae NM, Yoshinori H, et al. used Raman technology to obtain an accurate evaluation of the heart in vivo by examining cells in the myocardial infarction area of mice in different periods (Fig. 8) [181–184]. Niki T, Raffaele A, et al. used Raman to detect spectral changes in early stages of heart failure with preserved ejection fraction (HFPEF) (Fig. 9B), finding significant differences in the intensity ratios of Raman spectra within the four chambers of the heart [188]. Moreover, SERS has been used to measure the concentration of digoxin, a heart failure drug, in the blood to maximize its efficacy. This shows the potential of Raman detection of the therapeutic effect. Besides the application to common cardiovascular diseases, Raman also contributes to some rare cardiovascular diseases, like Fabry heart disease, a X-linked glycolipid metabolic disorder. In the study by Elen T, Nairveen A, et al., intracardiac lipid changes were detected by CARS [186]. Additionally, Yang Y, Rui S, Xiaojiang Y et al. have used Raman to detect miRNAs in patients with atrial fibrillation associated rheumatic mitral valve disease (RMVD), highlighting its potential in diagnosing RMVD and atrial fibrillation [187]. Furthermore, Raman has also been used to detect the thoracic aortic aneurysm in mice (Fig. 9C) [189].

The common clinical methods for detecting coronary heart disease are such as electrocardiograms (ECG), myocardial enzyme test, echocardiography and CTA [189, 190]. We have compared CTA with Raman in a previous section. ECG is a short-term method which can only check the electrical activity of the heart in a short time [191, 192]. The various myocardial enzymes have their own window periods that exceeding them can result in reduced detection efficacy or failure to detect [193]. Moreover, different myocardial enzymes have different specificities and sensitivities. Echocardiography is not sensitive enough to detect small areas of infarction. Additionally, it cannot visualize the coronary arteries themselves, but can only infer their presence and function based on the movement of the heart muscle [194]. Raman spectroscopy has the advantages of fast detection speed, high accuracy and the ability to detect specific sites, even the chemical composition of the infarcted area. This shows that Raman has great potential for clinical detection of myocardial infarction [195]. After comparison, Raman spectroscopy has the potential to play an important role in the diagnosis, evaluation of treatment efficacy, and prognosis of cardiovascular diseases. We provide an overview of the main application scope of Raman in cardiovascular diseases in Fig. 10.

Conclusion

Due to the constraints of length and depth, it is not feasible for us to delve into the specifics of all imaging techniques at various levels. However, we have elaborated on the unique characteristics of Raman that are not found in other traditional imaging techniques. Raman spectroscopy is a powerful optical technique owing to its label-free, high resolution, and non-invasive. This technology offers the advantage of the near real-time detection, high sensitivity and specificity. Raman spectroscopy is particularly useful for studying living cells as it does not require the use of markers that may damage cells. Additionally, living cell imaging can be performed in water-based conditions, allowing for imaging in phosphate buffer solutions or media without immobilization. These advantages highlight the great potential of Raman technology for clinical applications. This technology possesses significant potential through its integration with the recently emerging artificial intelligence (AI) technologies. AI-based algorithms are capable of substantially enhancing the accuracy and efficiency of spectral interpretation. This synergistic effect is expected to greatly improve the efficiency and precision of clinical diagnostics, as well as facilitate the innovation and application of novel diagnostic and therapeutic methodologies.

Author contributions Songcai X.: Conceptualization, Methodology, Software, Supervision, Writing- Original draft preparation, Writing- Reviewing and Editing. Xiaotong Z.: Writing- Reviewing and Editing. Feiyuan H.: Writing- Reviewing and Editing. Shengyuan W.: Writing- Reviewing and Editing. Kexin C.: Writing- Reviewing and Editing. Jing X.: Writing- Reviewing and Editing. Xiangwen X.: Conceptualization, Methodology, Writing- Reviewing and Editing . Chengyu S.: Writing- Reviewing and Editing. Shuo L.: Writing- Reviewing and Editing. Fan W.: Writing- Reviewing and Editing. Jinwei T.: Supervision, Funding acquisition, Project administration, Writing- Reviewing and Editing.

Funding This work receives the following funding: National Natural Science Foundation of China (82370343, U21A20391, 81971715, and 82100529), Natural Science Foundation of Heilongjiang Province of China (ZD2023H005), Fok Ying-Tong Education Foundation for Young Teachers (171032), Heilongjiang Applied Technology Research and Development Plan (GA20C007), HMU Marshal Initiative Funding (HMUMIF-21020) Key Laboratory of Emergency and Trauma of Ministry of Education (Hainan Medical University) (KLET-202117).

Data availability No datasets were generated or analysed during the current study.

Declarations

Ethics approval and consent to participate Not applicable.

Consent for publication All authors consent to the publication of this manuscript.

Competing interests The authors declare no competing interests.

References

1. Mittal R, Jhaveri VM, Kay SS, Greer A, Sutherland KJ, McMurry HS, Lin N, Mittal J, Malhotra AK, Patel AP (2019) Recent advances in understanding the Pathogenesis of Cardiovascular diseases and Development of Treatment modalities. Cardiovasc Hematol Disord Drug Targets 19(1):19–32. https://doi.org/10.2174/1871529x18666180508111353
2. Kumar V, Brent JR, Shorie M, Kaur H, Chadha G, Thomas AG, Lewis EA, Rooney AP, Nguyen L, Zhong XL, Burke MG, Haigh SJ, Walton A, McNaughter PD, Tedstone AA, Savjani N, Muryn CA, O'Brien P, Ganguli AK, Sabherwal P (2016) Nanostructured Aptamer-Functionalized Black Phosphorus sensing platform for Label-Free Detection of Myoglobin, a Cardiovascular Disease Biomarker. ACS Appl Mater Interfaces 8(35):22860–22868. https://doi.org/10.1021/acsami.6b06488
3. Mendis S, Puska P, Norrving B (2011) & WH., O. Global atlas on cardiovascular disease prevention and control. https://www.who.int/publications/i/item/9789241564373. Accessed 1 Nov 2024
4. Coats AJS, Anker SD, Baumbach A, Alfieri O, von Bardeleben RS, Bauersachs J, Bax JJ, Boveda S, Čelutkienė J, Cleland JG, Dagres N, Deneke T, Farmakis D, Filippatos G, Hausleiter J, Hindricks G, Jankowska EA, Lainscak M, Leclercq C, Prendergast B (2021) The management of secondary mitral regurgitation in patients with heart failure: a joint position statement from the Heart Failure Association (HFA), European Association of Cardiovascular Imaging (EACVI), European Heart Rhythm Association (EHRA), and European Association of Percutaneous Cardiovascular Interventions (EAPCI) of the ESC. Eur Heart J 42(13):1254–1269. https://doi.org/10.1093/eurheartj/ehab086
5. Noubiap JJ, Nyaga UF (2023) Cardiovascular disease prevention should start in early life. BMC Glob Public Health 1(1):14. https://doi.org/10.1186/s44263-023-00015-4
6. MacRitchie N, Grassia G, Noonan J, Garside P, Graham D, Maffia P (2018) Molecular imaging of atherosclerosis: spotlight on Raman spectroscopy and surface-enhanced Raman scattering. Heart 104(6):460–467. https://doi.org/10.1136/heartjnl-2017-311447
7. Kwak BR, Bäck M, Bochaton-Piallat ML, Caligiuri G, Daemens M, Davies PF, Hoefer IE, Holvoet P, Jo H, Krams R, Lehoux S, Monaco C, Steffens S, Virmani R, Weber C, Wentzel JJ, Evans PC (2014) Biomechanical factors in atherosclerosis: mechanisms and clinical implications. Eur Heart J 35(43):3013–. https://doi.org/10.1093/eurheartj/ehu353
8. Casscells W, Naghavi M, Willerson JT (2003) Vulnerable atherosclerotic plaque: a multifocal disease. Circulation 107(16):2072–2075. https://doi.org/10.1161/01.Cir.0000069329.70061.68
9. Libby P, Ridker PM, Maseri A (2002) Inflammation and atherosclerosis. Circulation 105(9):1135–1143. https://doi.org/10.1161/hc0902.104353
10. Shah PK (2002) Pathophysiology of coronary thrombosis: role of plaque rupture and plaque erosion. Prog Cardiovasc Dis 44(5):357–368. https://doi.org/10.1053/pcad.2002.123473
11. Shah PK (2003) Mechanisms of plaque vulnerability and rupture. J Am Coll Cardiol, 41(4 Suppl S), 15s-22s. https://doi.org/10.1016/s0735-1097(02)02834-6
12. Stary HC, Chandler AB, Dinsmore RE, Fuster V, Glagov S, Insull W Jr., Rosenfeld ME, Schwartz CJ, Wagner WD, Wissler RW (1995) A definition of advanced types of atherosclerotic lesions and a histological classification of atherosclerosis. A report from the Committee on Vascular Lesions of the Council on Arteriosclerosis. Am Heart Association Circulation 92(5):1355–1374. https://doi.org/10.1161/01.cir.92.5.1355
13. Aronson D, Rayfield EJ (2002) How hyperglycemia promotes atherosclerosis: molecular mechanisms. Cardiovasc Diabetol 1(1):1. https://doi.org/10.1186/1475-2840-1-1
14. Bergheanu SC, Bodde MC, Jukema JW (2017) Pathophysiology and treatment of atherosclerosis: current view and future perspective on lipoprotein modification treatment. Neth Heart J 25(4):231–242. https://doi.org/10.1007/s12471-017-0959-2
15. Björkegren JLM, Lusis AJ (2022) Atherosclerosis: recent developments. Cell 185(10):1630–1645. https://doi.org/10.1016/j.cell.2022.04.004
16. Tian Y, Deng P, Li B, Wang J, Li J, Huang Y, Zheng Y (2019) Treatment models of cardiac rehabilitation in patients with coronary heart disease and related factors affecting patient compliance. Rev Cardiovasc Med 20(1):27–33. https://doi.org/10.31083/j.rcm.2019.01.53
17. Passos LSA, Nunes MCP, Aikawa E (2020) Rheumatic Heart Valve Disease Pathophysiology and underlying mechanisms. Front Cardiovasc Med 7:612716. https://doi.org/10.3389/fcvm.2020.612716
18. Jun C, Fang B (2021) Current progress of fluoroquinolones-increased risk of aortic aneurysm and dissection. BMC Cardiovasc Disord 21(1):470. https://doi.org/10.1186/s12872-021-02258-1
19. Corrigendum to (2021) 2020 ESC guidelines on sports Cardiology and Exercise in patients with Cardiovascular Disease. Eur Heart J 42(5):548–549. https://doi.org/10.1093/eurheartj/ehaa835
20. Ozaki Y, Okumura M, Ismail TF, Motoyama S, Naruse H, Muramatsu T, Kawai H, Sarai M, Narula J (2015) The role of multiple imaging modalities to disclose the mechanism of ACS Angioscopy in comparison to other Imaging modalities including OCT, IVUS and CTA. In: Mizuno K, Takano M (eds) Coronary angioscopy. Springer Japan, pp 13–29. https://doi.org/10.1007/978-4-431-55546-9_2
21. Kapoor M, Kasi A (2024) PET scanning. In StatPearls. StatPearls Publishing Copyright © 2024. StatPearls Publishing LLC
22. Hawkins R (2023) Principles of Magnetic Resonance Imaging (MRI). In S. Tolofari, D. Moon, B. Starmer, & S. Payne (Eds.), Imaging and Technology in Urology (pp. 83–87). Springer International Publishing. https://doi.org/10.1007/978-3-031-26058-2_14

23. Ono M, Kawashima H, Hara H, Gao C, Wang R, Kogame N, Takahashi K, Chichareon P, Modolo R, Tomaniak M, Wykrzykowska JJ, Piek JJ, Mori I, Courtney BK, Wijns W, Sharif F, Bourantas C, Onuma Y, Serruys PW (2020) Advances in IVUS/OCT and future clinical perspective of Novel Hybrid Catheter System in Coronary Imaging. Front Cardiovasc Med 7:119. https://doi.org/10.3389/fcvm.2020.00119
24. Chaichi A, Prasad A, Gartia MR (2018) Raman Spectroscopy and Microscopy Applications in Cardiovascular diseases: from molecules to organs. Biosens (Basel) 8(4). https://doi.org/10.3390/bios8040107
25. Marcos-Vidal A, Marcos-Vidal A, Vaquero JJ, Vaquero JJ, Ripoll J, Ripoll J (2020) Optical Properties of Tissues in the Near Infrared. Their Relevance for Optical Bioimaging
26. Hang Y, Boryczka J, Wu N (2022) Visible-light and near-infrared fluorescence and surface-enhanced Raman scattering point-of-care sensing and bio-imaging: a review [10.1039/C9CS00621D]. Chem Soc Rev 51(1):329–375. https://doi.org/10.1039/C9CS00621D
27. Ngo NH, Nguyen AQ, Bufler FM, Kamakura Y, Mutoh H, Shimura T, Hosoi T, Watanabe H, Matagne P, Shimonomura K, Takehara K, Charbon E, Etoh TG (2020) Toward the super temporal resolution image Sensor with a Germanium Photodiode for visible light. Sens (Basel) 20(23). https://doi.org/10.3390/s20236895
28. Murty MVRK (1957) On the theoretical limit of Resolution. J Opt Soc Am 47(7):667–668. https://doi.org/10.1364/JOSA.47.000667
29. Patterson GH (2009) Fluorescence microscopy below the diffraction limit. Semin Cell Dev Biol 20(8):886–893. https://doi.org/10.1016/j.semcdb.2009.08.006
30. Paillet M, Meunier F, Verhaegen M, Blais-Ouellette S, Martel R (2010) High performance resonance Raman spectroscopy using volume Bragg gratings as tunable light filters. Rev Sci Instrum 81(5):053111. https://doi.org/10.1063/1.3405839
31. Sun Y, Li X, Galantu J, Chu Q, Chen J, Li F, Song N, Wang G, Ni Q (2023) Development of a Spatial Heterodyne Terahertz Raman Spectrometer with Echelle Gratings. Appl Sci, 13(2), 967. https://www.mdpi.com/2076-3417/13/2/967
32. Buckingham AD (1977) Raman spectroscopy. Nature 270(5636):458–458. https://doi.org/10.1038/270458b0
33. Jones RR, Hooper DC, Zhang L, Wolverson D, Valev VK (2019) Raman techniques: fundamentals and frontiers. Nanoscale Res Lett 14(1):231. https://doi.org/10.1186/s11671-019-3039-2
34. Orlando A, Franceschini F, Muscas C, Pidkova S, Bartoli M, Rovere M, Tagliaferro A (2021) A Comprehensive Review on Raman Spectroscopy Applications. Chemosensors, 9(9), 262. https://www.mdpi.com/2227-9040/9/9/262
35. Czamara K, Majzner K, Pacia MZ, Kochan K, Kaczor A, Baranska M (2015) Raman spectroscopy of lipids: a review. J Raman Spectrosc 46(1):4–20. https://doi.org/10.1002/jrs.4607
36. Lyon LA, Keating CD, Fox AP, Baker BE, He L, Nicewarner SR, Mulvaney SP, Natan MJ (1998) Raman spectroscopy. Anal Chem 70(12):341r–361r. https://doi.org/10.1021/a1980021p
37. Das RS, Agrawal YK (2011) Raman spectroscopy: recent advancements, techniques and applications. Vib Spectrosc 57(2):163–176. https://doi.org/10.1016/j.vibspec.2011.08.003
38. Wang N, Cao H, Wang L, Ren F, Zeng Q, Xu X, Liang J, Zhan Y, Chen X (2020) Recent advances in spontaneous Raman Spectroscopic Imaging: Instrumentation and Applications. Curr Med Chem 27(36):6188–6207. https://doi.org/10.2174/0929867326666190619114431
39. Rygula A, Majzner K, Marzec KM, Kaczor A, Pilarczyk M, Baranska M (2013) Raman spectroscopy of proteins: a review. J Raman Spectrosc 44(8):1061–1076. https://doi.org/10.1002/jrs.4335
40. Andrews D (2014) Rayleigh Scattering and Raman Effect, Theory. In. https://doi.org/10.1016/B978-0-12-409547-2.11337-X
41. Saletnik A, Saletnik B, Puchalski C (2021) Overview of Popular Techniques of Raman Spectroscopy and their potential in the study of plant tissues. Molecules 26(6). https://doi.org/10.3390/molecules26061537
42. Langer J, Jimenez de Aberasturi D, Aizpurua J, Alvarez-Puebla RA, Auguié B, Baumberg JJ, Bazan GC, Bell SEJ, Boisen A, Brolo AG, Choo J, Cialla-May D, Deckert V, Fabris L, Faulds K, de García FJ, Goodacre R, Graham D, Haes AJ, Liz-Marzán LM (2020) Present and Future of Surface-enhanced Raman Scattering. ACS Nano 14(1):28–117. https://doi.org/10.1021/acsnano.9b04224
43. Ouyang L, Ren W, Zhu L, Irudayaraj J (2017) Prosperity to challenges: recent approaches in SERS substrate fabrication. Rev Anal Chem 36(1). https://doi.org/10.1515/revac-2016-0027
44. Siebe HS, Chen Q, Li X, Xu Y, Browne WR, Bell SEJ (2021) Filter paper based SERS substrate for the direct detection of analytes in complex matrices [10.1039/D0AN02103B]. Analyst 146(4):1281–1288. https://doi.org/10.1039/D0AN02103B
45. Rodrigues MS, Borges J, Lopes C, Pereira RMS, Vasilevskiy MI, Vaz F (2021) Gas Sensors Based on Localized Surface Plasmon Resonances: Synthesis of Oxide Films with Embedded Metal Nanoparticles, Theory and Simulation, and Sensitivity Enhancement Strategies. Appl Sci, 11(12), 5388. https://www.mdpi.com/2076-3417/11/12/5388
46. Kulakovich OS, Gaponenko SV, Guzatov DV (2023) Metal–dielectric nanostructures for enhancement of molecular fluorescence. J Appl Spectrosc 90(3):567–575. https://doi.org/10.1007/s10812-023-01567-x
47. Chen Y-T, Pan L, Horneber A, van den Berg M, Miao P, Xu P, Adam P-M, Meixner AJ, Zhang D (2019) Charge transfer and electromagnetic enhancement processes revealed in the SERS and TERS of a CoPc thin film. Nanophotonics 8:1533–1546
48. Peng Y, Lin C, Long L, Masaki T, Tang M, Yang L, Liu J, Huang Z, Li Z, Luo X, Lombardi JR, Yang Y (2021) Charge-transfer resonance and electromagnetic enhancement synergistically enabling MXenes with excellent SERS sensitivity for SARS-CoV-2 S protein detection. Nanomicro Lett 13:52. https://doi.org/10.1007/s40820-020-00565-4
49. Wei H, Xu H (2013) Hot spots in different metal nanostructures for plasmon-enhanced Raman spectroscopy [10.1039/C3NR02924G]. Nanoscale 5(22):10794–10805. https://doi.org/10.1039/C3NR02924G
50. Maher RC (2012) SERS Hot spots. In: Kumar CSSR (ed) Raman Spectroscopy for nanomaterials characterization. Springer, Berlin Heidelberg, pp 215–260. https://doi.org/10.1007/978-3-642-20620-7_10
51. Li C, Huang Y, Li X, Zhang Y, Chen Q, Ye Z, Alqarni Z, Bell SEJ, Xu Y (2021) Towards practical and sustainable SERS: a review of recent developments in the construction of multifunctional enhancing substrates [10.1039/D1TC02134F]. J Mater Chem C 9(35):11517–11552. https://doi.org/10.1039/D1TC02134F
52. Ma J, Sun M (2020) Nonlinear optical microscopies (NOMs) and plasmon-enhanced NOMs for biology and 2D materials. Nanophotonics 9(6):1341–1358. https://doi.org/10.1515/nanoph-2020-0082
53. Eesley GL (1979) Coherent raman spectroscopy. J Quant Spectrosc Radiat Transf 22(6):507–576. https://doi.org/10.1016/0022-4073(79)90045-1
54. Freudiger CW, Min W, Saar BG, Lu S, Holtom GR, He C, Tsai JC, Kang JX, Xie XS (2008) Label-Free Biomedical Imaging with High Sensitivity by Stimulated Raman scattering Microscopy. Science 322(5909):1857–1861. https://doi.org/10.1126/science.1165758

55. Wei L, Yu Y, Shen Y, Wang MC, Min W (2013) Vibrational imaging of newly synthesized proteins in live cells by stimulated Raman scattering microscopy. Proc Natl Acad Sci U S A 110(28):11226–11231. https://doi.org/10.1073/pnas.1303768110
56. Moore S D. (2013) Ji-Xin Cheng and Xiaoliang Sunney Xie (eds.): Coherent Raman scattering microscopy. Anal Bioanal Chem 405(15):5001–5002. https://doi.org/10.1007/s00216-013-6861-x
57. Duncan MD, Reintjes J, Manuccia TJ (1982) Scanning coherent anti-stokes Raman microscope. Opt Lett 7(8):350–352. https://doi.org/10.1364/OL.7.000350
58. Zumbusch A, Holtom GR, Xie XS (1999) Three-dimensional vibrational imaging by coherent Anti-stokes Raman Scattering. Phys Rev Lett 82(20):4142–4145. https://doi.org/10.1103/PhysRevLett.82.4142
59. Müller M, Schins JM (2002) Imaging the thermodynamic state of lipid membranes with Multiplex CARS Microscopy. J Phys Chem B 106:3715–3723
60. Kano H, Hamaguchi H-o (2005) Vibrationally resonant imaging of a single living cell by supercontinuum-based multiplex coherent anti-stokes Raman scattering microspectroscopy. Opt Express 13(4):1322–1327. https://doi.org/10.1364/OPEX.13.001322
61. Hirai N, Maeda Y, Hashimoto K, Andriana BB, Matsuyoshi H, Sato H (2021) Coherent anti-stokes Raman scattering Spectroscopy using a double-Wavelength-Emission electronically tuned Ti:Sapphire Laser. Appl Spectrosc 75(8):988–993. https://doi.org/10.1177/00037028211020313
62. Le TT, Yue S, Cheng JX (2010) Shedding new light on lipid biology with coherent anti-stokes Raman scattering microscopy. J Lipid Res 51(11):3091–3102. https://doi.org/10.1194/jlr.R008730
63. Serebrennikova KV, Berlina AN, Sotnikov DV, Zherdev AV, Dzantiev BB (2021) Raman Scattering-Based Biosensing: new prospects and opportunities. Biosens (Basel) 11(12). https://doi.org/10.3390/bios11120512
64. Shipp DW, Sinjab F, Notingher I (2017) Raman spectroscopy: techniques and applications in the life sciences. Adv Opt Photonics 9(2):315–428. https://doi.org/10.1364/AOP.9.000315
65. Wang H, Liu Y, Rao G, Wang Y, Du X, Hu A, Hu Y, Gong C, Wang X, Xiong J (2021) Coupling enhancement mechanisms, materials, and strategies for surface-enhanced Raman scattering devices [10.1039/D1AN00624J]. Analyst 146(16):5008–5032. https://doi.org/10.1039/D1AN00624J
66. Zong C, Premasiri R, Lin H, Huang Y, Zhang C, Yang C, Ren B, Ziegler LD, Cheng J-X (2019) Plasmon-enhanced stimulated Raman scattering microscopy with single-molecule detection sensitivity. Nat Commun 10(1):5318. https://doi.org/10.1038/s41467-019-13230-1
67. Zhang C, Zhang D, Cheng JX (2015) Coherent Raman Scattering Microscopy in Biology and Medicine. Annu Rev Biomed Eng 17:415–445. https://doi.org/10.1146/annurev-bioeng-071114-040554
68. Folick A, Min W, Wang MC (2011) Label-free imaging of lipid dynamics using coherent anti-stokes Raman Scattering (CARS) and stimulated Raman Scattering (SRS) microscopy. Curr Opin Genet Dev 21(5):585–590. https://doi.org/10.1016/j.gde.2011.09.003
69. Tipping WJ, Lee M, Serrels A, Brunton VG, Hulme AN (2016) Stimulated Raman scattering microscopy: an emerging tool for drug discovery. Chem Soc Rev 45(8):2075–2089. https://doi.org/10.1039/c5cs00693g
70. Doris MK, Dweck MR, Fayad ZA (2016) The future of imaging in cardiovascular disease intervention trials: 2017 and beyond. Curr Opin Lipidol 27(6):605–614. https://doi.org/10.1097/mol.0000000000000350
71. Jafari M, Shoeibi A, Khodatars M, Ghassemi N, Moridian P, Alizadehsani R, Khosravi A, Ling SH, Delfan N, Zhang YD, Wang SH, Gorriz JM, Alinejad-Rokny H, Acharya UR (2023) Automated diagnosis of cardiovascular diseases from cardiac magnetic resonance imaging using deep learning models: a review. Comput Biol Med 160:106998. https://doi.org/10.1016/j.compbiomed.2023.106998
72. Stanton EH, Persson N, Gomolka RS, Lilius T, Sigurðsson B, Lee H, Xavier ALR, Benveniste H, Nedergaard M, Mori Y (2021) Mapping of CSF transport using high spatiotemporal resolution dynamic contrast-enhanced MRI in mice: Effect of anesthesia. Magn Reson Med 85(6):3326–3342. https://doi.org/10.1002/mrm.28645
73. Hartley A, Haskard D, Khamis R (2019) Oxidized LDL and anti-oxidized LDL antibodies in atherosclerosis - novel insights and future directions in diagnosis and therapy<sup/>. Trends Cardiovasc Med 29(1):22–26. https://doi.org/10.1016/j.tcm.2018.05.010
74. Tsimikas S, Willeit P, Willeit J, Santer P, Mayr M, Xu Q, Mayr A, Witztum JL, Kiechl S (2012) Oxidation-specific biomarkers, prospective 15-year cardiovascular and stroke outcomes, and net reclassification of cardiovascular events. J Am Coll Cardiol 60(21):2218–2229. https://doi.org/10.1016/j.jacc.2012.08.979
75. Gao S, Zhao D, Wang M, Zhao F, Han X, Qi Y, Liu J (2017) Association between circulating oxidized LDL and atherosclerotic Cardiovascular Disease: a Meta-analysis of Observational studies. Can J Cardiol 33(12):1624–1632. https://doi.org/10.1016/j.cjca.2017.07.015
76. Palinski W, Hörkkö S, Miller E, Steinbrecher UP, Powell HC, Curtiss LK, Witztum JL (1996) Cloning of monoclonal autoantibodies to epitopes of oxidized lipoproteins from apolipoprotein E-deficient mice. Demonstration of epitopes of oxidized low density lipoprotein in human plasma. J Clin Invest 98(3):800–814. https://doi.org/10.1172/jci118853
77. Tsimikas S, Shortal BP, Witztum JL, Palinski W (2000) In vivo uptake of radiolabeled MDA2, an oxidation-specific monoclonal antibody, provides an accurate measure of atherosclerotic lesions rich in oxidized LDL and is highly sensitive to their regression. Arterioscler Thromb Vasc Biol 20(3):689–697. https://doi.org/10.1161/01.atv.20.3.689
78. Tsimikas S (2002) Noninvasive imaging of oxidized low-density lipoprotein in atherosclerotic plaques with tagged oxidation-specific antibodies. Am J Cardiol 90(10c):22l–27l. https://doi.org/10.1016/s0002-9149(02)02958-2
79. Briley-Saebo KC, Nguyen TH, Saeboe AM, Cho YS, Ryu SK, Volkova ER, Dickson S, Leibundgut G, Wiesner P, Green S, Casanada F, Miller YI, Shaw W, Witztum JL, Fayad ZA, Tsimikas S (2012) In vivo detection of oxidation-specific epitopes in atherosclerotic lesions using biocompatible manganese molecular magnetic imaging probes. J Am Coll Cardiol 59(6):616–626. https://doi.org/10.1016/j.jacc.2011.10.881
80. Adrian M (2005) MRI: understanding its limitations. Br Columb Med J 47:359–361
81. Natalin RA, Prince MR, Grossman ME, Silvers D, Landman J (2010) Contemporary applications and limitations of magnetic resonance imaging contrast materials. J Urol 183(1):27–33. https://doi.org/10.1016/j.juro.2009.09.029
82. Kooi ME, Cappendijk VC, Cleutjens KB, Kessels AG, Kitslaar PJ, Borgers M, Frederik PM, Daemen MJ, van Engelshoven JM (2003) Accumulation of Ultrasmall superparamagnetic particles of iron oxide in human atherosclerotic plaques can be detected by in vivo magnetic resonance imaging. Circulation 107(19):2453–2458. https://doi.org/10.1161/01.Cir.0000068315.98705.Cc
83. Ruehm SG, Corot C, Vogt P, Kolb S, Debatin JF (2001) Magnetic resonance imaging of atherosclerotic plaque with ultrasmall superparamagnetic particles of iron oxide in hyperlipidemic

rabbits. Circulation 103(3):415–422. https://doi.org/10.1161/01.cir.103.3.415
84. Noonan J, Asiala SM, Grassia G, MacRitchie N, Gracie K, Carson J, Moores M, Girolami M, Bradshaw AC, Guzik TJ, Meehan GR, Scales HE, Brewer JM, McInnes IB, Sattar N, Faulds K, Garside P, Graham D, Maffia P (2018) In vivo multiplex molecular imaging of vascular inflammation using surface-enhanced Raman spectroscopy. Theranostics 8(22):6195–6209. https://doi.org/10.7150/thno.28665
85. van Sluis J, de Jong J, Schaar J, Noordzij W, van Snick P, Dierckx R, Borra R, Willemsen A, Boellaard R (2019) Performance characteristics of the Digital Biograph Vision PET/CT system. J Nucl Med 60(7):1031–1036. https://doi.org/10.2967/jnumed.118.215418
86. Townsend DW, Carney JP, Yap JT, Hall NC (2004) PET/CT today and tomorrow. J Nucl Med 45(Suppl 1):4s–14s
87. Celeng C, de Keizer B, Merkely B, de Jong P, Leiner T, Takx RAP (2018) PET molecular targets and Near-Infrared fluorescence imaging of atherosclerosis. Curr Cardiol Rep 20(2):11. https://doi.org/10.1007/s11886-018-0953-3
88. Sriranjan RS, Tarkin JM, Evans NR, Le EPV, Chowdhury MM, Rudd JH F (2021) Atherosclerosis imaging using PET: insights and applications. Br J Pharmacol 178(11):2186–2203. https://doi.org/10.1111/bph.14868
89. Hiari N, Rudd JH (2011) FDG PET imaging and cardiovascular inflammation. Curr Cardiol Rep 13(1):43–48. https://doi.org/10.1007/s11886-010-0150-5
90. Tarkin JM, Joshi FR, Rudd JH (2014) PET imaging of inflammation in atherosclerosis. Nat Rev Cardiol 11(8):443–457. https://doi.org/10.1038/nrcardio.2014.80
91. Senders ML, Calcagno C, Tawakol A, Nahrendorf M, Mulder WJM, Fayad ZA (2023) PET/MR imaging of inflammation in atherosclerosis. Nat Biomed Eng 7(3):202–220. https://doi.org/10.1038/s41551-022-00970-7
92. Raynor WY, Park PSU, Borja AJ, Sun Y, Werner TJ, Ng SJ, Lau HC, Høilund-Carlsen PF, Alavi A, Revheim ME (2021) PET-Based imaging with (18)F-FDG and (18)F-NaF to assess inflammation and microcalcification in atherosclerosis and other Vascular and Thrombotic disorders. Diagnostics (Basel) 11(12). https://doi.org/10.3390/diagnostics11122234
93. Reubi JC, Schär JC, Waser B, Wenger S, Heppeler A, Schmitt JS, Mäcke HR (2000) Affinity profiles for human somatostatin receptor subtypes SST1-SST5 of somatostatin radiotracers selected for scintigraphic and radiotherapeutic use. Eur J Nucl Med 27(3):273–282. https://doi.org/10.1007/s002590050034
94. Tarkin JM, Joshi FR, Evans NR, Chowdhury MM, Figg NL, Shah AV, Starks LT, Martin-Garrido A, Manavaki R, Yu E, Kuc RE, Grassi L, Kreuzhuber R, Kostadima MA, Frontini M, Kirkpatrick PJ, Coughlin PA, Gopalan D, Fryer TD, Rudd JH (2017) Detection of atherosclerotic inflammation by (68)Ga-DOTATATE PET compared to [(18)F]FDG PET Imaging. J Am Coll Cardiol 69(14):1774–1791. https://doi.org/10.1016/j.jacc.2017.01.060
95. Gourni E, Demmer O, Schottelius M, D'Alessandria C, Schulz S, Dijkgraaf I, Schumacher U, Schwaiger M, Kessler H, Wester HJ (2011) PET of CXCR4 expression by a (68)Ga-labeled highly specific targeted contrast agent. J Nucl Med 52(11):1803–1810. https://doi.org/10.2967/jnumed.111.098798
96. Weiberg D, Thackeray JT, Daum G, Sohns JM, Kropf S, Wester HJ, Ross TL, Bengel FM, Derlin T (2018) Clinical molecular imaging of chemokine receptor CXCR4 expression in atherosclerotic plaque using (68)Ga-Pentixafor PET: correlation with Cardiovascular Risk factors and calcified plaque burden. J Nucl Med 59(2):266–272. https://doi.org/10.2967/jnumed.117.196485
97. Huet P, Burg S, Le Guludec D, Hyafil F, Buvat I (2015) Variability and uncertainty of 18F-FDG PET imaging protocols for assessing inflammation in atherosclerosis: suggestions for improvement. J Nucl Med 56(4):552–559. https://doi.org/10.2967/jnumed.114.142596
98. Anton-Rodriguez JM, Julyan PJ, Djoukhadar I, Russell D, Evans DG, Jackson A, Matthews JC (2019) Comparison of a Standard Resolution PET-CT scanner with an HRRT Brain scanner for imaging small tumors within the Head. IEEE T RADIAT PLASMA 3:434–443
99. Blomberg BA, Thomassen A, Takx RA, Hildebrandt MG, Simonsen JA, Buch-Olsen KM, Diederichsen AC, Mickley H, Alavi A, Høilund-Carlsen PF (2014) Delayed ^{18}F-fluorodeoxyglucose PET/CT imaging improves quantitation of atherosclerotic plaque inflammation: results from the CAMONA study. J Nucl Cardiol 21(3):588–597. https://doi.org/10.1007/s12350-014-9884-6
100. Bateman TM (2012) Advantages and disadvantages of PET and SPECT in a busy clinical practice. J Nucl Cardiol 19(Suppl 1):3–11. https://doi.org/10.1007/s12350-011-9490-9
101. Nan X, Cheng JX, Xie XS (2003) Vibrational imaging of lipid droplets in live fibroblast cells with coherent anti-stokes Raman scattering microscopy. J Lipid Res 44(11):2202–2208. https://doi.org/10.1194/jlr.D300022-JLR200
102. Li L, Wang H, Cheng JX (2005) Quantitative coherent anti-stokes Raman scattering imaging of lipid distribution in coexisting domains. Biophys J 89(5):3480–3490. https://doi.org/10.1529/biophysj.105.065607
103. Ouimet M, Franklin V, Mak E, Liao X, Tabas I, Marcel YL (2011) Autophagy regulates cholesterol efflux from macrophage foam cells via lysosomal acid lipase. Cell Metab 13(6):655–667. https://doi.org/10.1016/j.cmet.2011.03.023
104. Robinet P, Ritchey B, Smith JD (2013) Physiological difference in autophagic flux in macrophages from 2 mouse strains regulates cholesterol ester metabolism. Arterioscler Thromb Vasc Biol 33(5):903–910. https://doi.org/10.1161/atvbaha.112.301041
105. Ouimet M, Ediriweera H, Afonso MS, Ramkhelawon B, Singaravelu R, Liao X, Bandler RC, Rahman K, Fisher EA, Rayner KJ, Pezacki JP, Tabas I, Moore KJ (2017) microRNA-33 regulates macrophage autophagy in atherosclerosis. Arterioscler Thromb Vasc Biol 37(6):1058–1067. https://doi.org/10.1161/atvbaha.116.308916
106. Matthäus C, Dochow S, Bergner G, Lattermann A, Romeike BF, Marple ET, Krafft C, Dietzek B, Brehm BR, Popp J (2012) In vivo characterization of atherosclerotic plaque depositions by Raman-probe spectroscopy and in vitro coherent anti-stokes Raman scattering microscopic imaging on a rabbit model. Anal Chem 84(18):7845–7851. https://doi.org/10.1021/ac301522d
107. Gottschall T, Meyer T, Baumgartl M, Dietzek B, Popp J, Limpert J, Tünnermann A (2014) Fiber-based optical parametric oscillator for high resolution coherent anti-stokes Raman scattering (CARS) microscopy. Opt Express 22(18):21921–21928. https://doi.org/10.1364/oe.22.021921
108. Ozeki Y, Umemura W, Otsuka Y, Satoh S, Hashimoto H, Sumimura K, Nishizawa N, Fukui K, Itoh K (2012) High-speed molecular spectral imaging of tissue with stimulated Raman scattering. Nat Photonics 6(12):845–851. https://doi.org/10.1038/nphoton.2012.263
109. Cheng JX, Jia YK, Zheng G, Xie XS (2002) Laser-scanning coherent anti-stokes Raman scattering microscopy and applications to cell biology. Biophys J 83(1):502–509. https://doi.org/10.1016/s0006-3495(02)75186-2
110. Stiebing C, Meyer T, Rimke I, Matthäus C, Schmitt M, Lorkowski S, Popp J (2017) Real-time Raman and SRS imaging of living human macrophages reveals cell-to-cell heterogeneity and dynamics of lipid uptake. J Biophotonics 10(9):1217–1226. https://doi.org/10.1002/jbio.201600279
111. Pallen S, Shetty Y, Das S, Vaz JM, Mazumder N (2021) Advances in nonlinear optical microscopy techniques for in vivo and in

vitro neuroimaging. Biophys Rev 13(6):1199–1217. https://doi.org/10.1007/s12551-021-00832-7
112. Li S, Li Y, Yi R, Liu L, Qu J (2020) Coherent anti-stokes Raman Scattering Microscopy and its applications. FRONT PHYS-LAUSANNE 8. https://doi.org/10.3389/fphy.2020.598420. [Review]
113. Balan V, Mihai CT, Cojocaru FD, Uritu CM, Dodi G, Botezat D, Gardikiotis I (2019) Vibrational spectroscopy fingerprinting in Medicine: from Molecular to Clinical Practice. Mater (Basel) 12(18). https://doi.org/10.3390/ma12182884
114. Sala A, Anderson DJ, Brennan PM, Butler HJ, Cameron JM, Jenkinson MD, Rinaldi C, Theakstone AG, Baker MJ (2020) Biofluid diagnostics by FTIR spectroscopy: a platform technology for cancer detection. Cancer Lett 477:122–130. https://doi.org/10.1016/j.canlet.2020.02.020
115. Wenning M, Scherer S, Naumann D, Diem M, Griffiths PCJ (2008) Vibrational Spectroscopy for Medical Diagnosis
116. Lasch P, Kneipp J (2008) Biomedical Vibrational Spectroscopy
117. Horsnell JD, Smith JA, Sattlecker M, Sammon A, Christie-Brown J, Kendall C, Stone N (2012) Raman spectroscopy–a potential new method for the intra-operative assessment of axillary lymph nodes. Surgeon 10(3):123–127. https://doi.org/10.1016/j.surge.2011.02.004
118. Shafer-Peltier K, Haka AS, Fitzmaurice M, Crowe JP, Myles JL, Dasari RR, Feld MS (2002) Raman microspectroscopic model of human breast tissue: implications for breast cancer diagnosis in vivo. J Raman Spectrosc 33:552–563
119. Manoharan R, Baraga JJ, Rava RP, Dasari RR, Fitzmaurice M, Feld MS (1993) Biochemical analysis and mapping of atherosclerotic human artery using FT-IR microspectroscopy. Atherosclerosis 103(2):181–193. https://doi.org/10.1016/0021-9150(93)90261-r
120. T PW, Mateuszuk L, Chlopicki S, Malek K, Baranska M (2011) Imaging of lipids in atherosclerotic lesion in aorta from ApoE/LDLR-/- mice by FT-IR spectroscopy and hierarchical cluster analysis. Analyst 136(24):5247–5255. https://doi.org/10.1039/c1an15311k
121. Lattermann A, Matthäus C, Bergner N, Beleites C, Romeike BF, Krafft C, Brehm BR, Popp J (2013) Characterization of atherosclerotic plaque depositions by Raman and FTIR imaging. J Biophotonics 6(1):110–121. https://doi.org/10.1002/jbio.201200146
122. Fels LE, Zamama M, Hafidi M (2015) Advantages and limitations of using FTIR Spectroscopy for assessing the Maturity of Sewage Sludge. and Olive Oil Waste Co-composts
123. Ali SM, Bonnier F, Lambkin HA, Flynn KM, McDonagh V, Healy C, Lee TC, Lyng FM, Byrne HJ (2013) A comparison of Raman, FTIR and ATR-FTIR micro spectroscopy for imaging human skin tissue sections. ANAL METHODS-UK 5:2281–2291
124. Le TT, Langohr IM, Locker MJ, Sturek M, Cheng JX (2007) Label-free molecular imaging of atherosclerotic lesions using multimodal nonlinear optical microscopy. J Biomed Opt 12(5):054007. https://doi.org/10.1117/1.2795437
125. Wang HW, Langohr IM, Sturek M, Cheng JX (2009) Imaging and quantitative analysis of atherosclerotic lesions by CARS-based multimodal nonlinear optical microscopy. Arterioscler Thromb Vasc Biol 29(9):1342–1348. https://doi.org/10.1161/atvbaha.109.189316
126. Kobat D, Durst ME, Nishimura N, Wong AW, Schaffer CB, Xu C (2009) Deep tissue multiphoton microscopy using longer wavelength excitation. Opt Express 17(16):13354–13364. https://doi.org/10.1364/oe.17.013354
127. Kim Y-i, Jeong S, Jun B-H, Lee Y-S, Lee Y-S, Jeong DH, Lee DS (2017) Endoscopic imaging using surface-enhanced Raman scattering. Eur J Nanomed 9:104–191
128. Gao L, Wang Z, Wong STC (2012) Use of coherent anti-stokes raman scattering (CARS) to meet the challenges of intraoperative imaging. Am Lab 44:10–15
129. Choudhury RP, Fuster V, Fayad ZA (2004) Molecular, cellular and functional imaging of atherothrombosis. Nat Rev Drug Discov 3(11):913–925. https://doi.org/10.1038/nrd1548
130. Tearney GJ, Brezinski ME, Bouma BE, Boppart SA, Pitris C, Southern JF, Fujimoto JG (1997) In vivo endoscopic optical biopsy with optical coherence tomography. Science 276(5321):2037–2039. https://doi.org/10.1126/science.276.5321.2037
131. Stamper DL, Weissman N, Brezinski ME (2006) Plaque characterization with optical coherence tomography. J Am Coll Cardiol 47(8 Suppl):C69–79
132. Reja SI, Minoshima M, Hori Y, Kikuchi K (2020) Near-infrared fluorescent probes: a next-generation tool for protein-labeling applications. Chem Sci 12(10):3437–3447. https://doi.org/10.1039/d0sc04792a
133. Huang J, Pu K (2020) Near-infrared fluorescent molecular probes for imaging and diagnosis of nephro-urological diseases. Chem Sci 12(10):3379–3392. https://doi.org/10.1039/d0sc02925d
134. Oörni K, Sneck M, Brömme D, Pentikäinen MO, Lindstedt KA, Mäyränpää M, Aitio H, Kovanen PT (2004) Cysteine protease cathepsin F is expressed in human atherosclerotic lesions, is secreted by cultured macrophages, and modifies low density lipoprotein particles in vitro. J Biol Chem 279(33):34776–34784. https://doi.org/10.1074/jbc.M310814200
135. Khraishah H, Jaffer FA (2020) Intravascular molecular imaging: Near-Infrared fluorescence as a New Frontier. Front Cardiovasc Med 7:587100 Published 2020 Nov 23. https://doi.org/10.3389/fcvm.2020.587100
136. Blomberg BA, Thomassen A, de Jong PA, Simonsen JA, Lam MG, Nielsen AL, Mickley H, Mali WP, Alavi A, Høilund-Carlsen PF (2015) Impact of personal characteristics and technical factors on quantification of Sodium 18F-Fluoride uptake in human arteries: prospective evaluation of healthy subjects. J Nucl Med 56(10):1534–1540. https://doi.org/10.2967/jnumed.115.159798
137. Jaffer FA, Vinegoni C, John MC, Aikawa E, Gold HK, Finn AV, Ntziachristos V, Libby P, Weissleder R (2008) Real-time catheter molecular sensing of inflammation in proteolytically active atherosclerosis. Circulation 118(18):1802–1809. https://doi.org/10.1161/circulationaha.108.785881
138. Jaffer FA, Calfon MA, Rosenthal A, Mallas G, Razansky RN, Mauskapf A, Weissleder R, Libby P, Ntziachristos V (2011) Two-dimensional intravascular near-infrared fluorescence molecular imaging of inflammation in atherosclerosis and stent-induced vascular injury. J Am Coll Cardiol 57(25):2516–2526. https://doi.org/10.1016/j.jacc.2011.02.036
139. Ughi GJ, Wang H, Gerbaud E, Gardecki JA, Fard AM, Hamidi E, Vacas-Jacques P, Rosenberg M, Jaffer FA, Tearney GJ (2016) Clinical characterization of coronary atherosclerosis with dual-modality OCT and Near-Infrared Autofluorescence Imaging. JACC Cardiovasc Imaging 9(11):1304–1314. https://doi.org/10.1016/j.jcmg.2015.11.020
140. Araki M, Park SJ, Dauerman HL, Uemura S, Kim JS, Di Mario C, Johnson TW, Guagliumi G, Kastrati A, Joner M, Holm NR, Alfonso F, Wijns W, Adriaenssens T, Nef H, Rioufol G, Amabile N, Souteyrand G, Meneveau N, Jang IK (2022) Optical coherence tomography in coronary atherosclerosis assessment and intervention. Nat Rev Cardiol 19(10):684–703. https://doi.org/10.1038/s41569-022-00687-9
141. Sinclair H, Bourantas C, Bagnall A, Mintz GS, Kunadian V (2015) OCT for the identification of vulnerable plaque in acute coronary syndrome. JACC Cardiovasc Imaging 8(2):198–209. https://doi.org/10.1016/j.jcmg.2014.12.005
142. Ali ZA, Maehara A, Généreux P, Shlofmitz RA, Fabbiocchi F, Nazif TM, Guagliumi G, Meraj PM, Alfonso F, Samady H, Akasaka T, Carlson EB, Leesar MA, Matsumura M, Ozan MO, Mintz GS, Ben-Yehuda O, Stone GW (2016) Optical coherence

tomography compared with intravascular ultrasound and with angiography to guide coronary stent implantation (ILUMIEN III: OPTIMIZE PCI): a randomised controlled trial. Lancet 388(10060):2618–2628. https://doi.org/10.1016/s0140-6736(16)31922-5
143. Ali ZA, Galougahi K, Mintz K, Maehara GS, Shlofmitz A, R. A., Mattesini A (2021) Intracoronary optical coherence tomography: state of the art and future directions. EuroIntervention 17(2):e105–e123. https://doi.org/10.4244/eij-d-21-00089
144. Dong N, Xie Z, Wang W, Dai J, Sun M, Pu Z, Tian J, Yu B (2016) Comparison of coronary arterial lumen dimensions on angiography and plaque characteristics on optical coherence tomography images and their changes induced by statin. BMC Med Imaging 16(1):63. https://doi.org/10.1186/s12880-016-0166-4
145. Phipps JE, Hoyt T, Vela D, Wang T, Michalek JE, Buja LM, Jang IK, Milner TE, Feldman MD (2016) Diagnosis of thin-capped Fibroatheromas in Intravascular Optical Coherence Tomography images: effects of Light Scattering. Circ Cardiovasc Interv 9(7). https://doi.org/10.1161/circinterventions.115.003163
146. Brezinski ME, Harjai KJ (2014) Current OCT approaches do not reliably identify TCFAs. J Clin Exp Cardiolog 5(11). https://doi.org/10.4172/2155-9880.1000350
147. Nissen SE, Yock P (2001) Intravascular ultrasound: novel pathophysiological insights and current clinical applications. Circulation 103(4):604–616. https://doi.org/10.1161/01.cir.103.4.604
148. Maehara A, Matsumura M, Ali ZA, Mintz GS, Stone GW (2017) IVUS-Guided Versus OCT-Guided coronary stent implantation: a critical Appraisal. JACC Cardiovasc Imaging 10(12):1487–1503. https://doi.org/10.1016/j.jcmg.2017.09.008
149. Mintz GS (2014) Clinical utility of intravascular imaging and physiology in coronary artery disease. J Am Coll Cardiol 64(2):207–222. https://doi.org/10.1016/j.jacc.2014.01.015
150. Dong L, Jiang W, Lu W, Jiang J, Zhao Y, Song X, Leng X, Zhao H, Wang J, Li C, Xiang J (2021) Automatic segmentation of coronary lumen and external elastic membrane in intravascular ultrasound images using 8-layer U-Net. Biomed Eng Online 20(1):16. https://doi.org/10.1186/s12938-021-00852-0
151. Luo T, Wischgoll T, Kwon Koo B, Huo Y, Kassab GS (2014) IVUS validation of patient coronary artery lumen area obtained from CT images. PLoS ONE 9(1):e86949. https://doi.org/10.1371/journal.pone.0086949
152. Broersen A, de Graaf MA, Eggermont J, Wolterbeek R, Kitslaar PH, Dijkstra J, Bax JJ, Reiber JH, Scholte AJ (2016) Enhanced characterization of calcified areas in intravascular ultrasound virtual histology images by quantification of the acoustic shadow: validation against computed tomography coronary angiography. Int J Cardiovasc Imaging 32(4):543–552. https://doi.org/10.1007/s10554-015-0820-x
153. Suh WM, Seto AH, Margey RJ, Cruz-Gonzalez I, Jang IK (2011) Intravascular detection of the vulnerable plaque. Circ Cardiovasc Imaging 4(2):169–178. https://doi.org/10.1161/circimaging.110.958777
154. Natesan S, Mosarla RC, Parikh SA, Rosenfield K, Suomi J, Chalyan D, Jaff M, Secemsky EA (2022) Intravascular ultrasound in peripheral venous and arterial interventions: a contemporary systematic review and grading of the quality of evidence. Vasc Med 27(4):392–400. https://doi.org/10.1177/1358863x221092817
155. Arrey-Mbi TB, Klusewitz SM, Villines TC (2017) Long-term Prognostic Value of Coronary computed Tomography Angiography. Curr Treat Options Cardiovasc Med 19(12):90. https://doi.org/10.1007/s11936-017-0588-5
156. Thomas DM, Divakaran S, Villines TC, Nasir K, Shah NR, Slim AM, Blankstein R, Cheezum MK (2015) Management of coronary artery calcium and coronary CTA findings. Curr Cardiovasc Imaging Rep 8(6):18. https://doi.org/10.1007/s12410-015-9334-0
157. Li Y, Wu Y, He J, Jiang W, Wang J, Peng Y, Jia Y, Xiong T, Jia K, Yi Z, Chen M (2022) Automatic coronary artery segmentation and diagnosis of stenosis by deep learning based on computed tomographic coronary angiography. Eur Radiol 32(9):6037–6045. https://doi.org/10.1007/s00330-022-08761-z
158. Abbara S, Blanke P, Maroules CD, Cheezum M, Choi AD, Han BK, Marwan M, Naoum C, Norgaard BL, Rubinshtein R, Schoenhagen P, Villines T, Leipsic J (2016) SCCT guidelines for the performance and acquisition of coronary computed tomographic angiography: a report of the society of Cardiovascular computed Tomography Guidelines Committee: endorsed by the North American Society for Cardiovascular Imaging (NASCI). J Cardiovasc Comput Tomogr 10(6):435–449. https://doi.org/10.1016/j.jcct.2016.10.002
159. Glagov S, Weisenberg E, Zarins CK, Stankunavicius R, Kolettis GJ (1987) Compensatory enlargement of human atherosclerotic coronary arteries. N Engl J Med 316(22):1371–1375. https://doi.org/10.1056/nejm198705283162204
160. Nissen SE, Gurley JC (1991) Application of intravascular ultrasound for detection and quantitation of coronary atherosclerosis. Int J Card Imaging 6(3–4):165–177. https://doi.org/10.1007/bf01797849
161. Grondin CM, Dyrda I, Pasternac A, Campeau L, Bourassa MG, Lespérance J (1974) Discrepancies between cineangiographic and postmortem findings in patients with coronary artery disease and recent myocardial revascularization. Circulation 49(4):703–708. https://doi.org/10.1161/01.cir.49.4.703
162. Matter CM, Stuber M, Nahrendorf M (2009) Imaging of the unstable plaque: how far have we got? Eur Heart J 30(21):2566–2574. https://doi.org/10.1093/eurheartj/ehp419
163. Liu Y, Liao Q, Zhang N, Dong X, Ullah N, Wang Y, Li X, Huang L (2023) Raman Spectroscopy Fiber Probe based on metalens and Multimode Fiber for Malachite Green determination. IEEE SENS J 23(15):16866–16872. https://doi.org/10.1109/JSEN.2023.3284889
164. Stevens O, Iping Petterson IE, Day JC, Stone N (2016) Developing fibre optic Raman probes for applications in clinical spectroscopy. Chem Soc Rev 45(7):1919–1934. https://doi.org/10.1039/c5cs00850f
165. Buschman HP, Marple ET, Wach ML, Bennett B, Schut TC, Bruining HA, Bruschke AV, van der Laarse A, Puppels GJ (2000) In vivo determination of the molecular composition of artery wall by intravascular Raman spectroscopy. Anal Chem 72(16):3771–3775. https://doi.org/10.1021/ac000298b
166. Motz JT, Fitzmaurice M, Miller A, Gandhi SJ, Haka AS, Galindo LH, Dasari RR, Kramer JR, Feld MS (2006) In vivo Raman spectral pathology of human atherosclerosis and vulnerable plaque. J Biomed Opt 11(2):021003. https://doi.org/10.1117/1.2190967
167. Xi X, Liang C (2021) Perspective of future SERS Clinical Application based on current status of Raman Spectroscopy clinical trials. Front Chem 9:665841. https://doi.org/10.3389/fchem.2021.665841
168. Li B, Ding H, Wang Z, Liu Z, Cai X, Yang H (2022) Research on the difference between patients with coronary heart disease and healthy controls by surface enhanced Raman spectroscopy. Spectrochim Acta Mol Biomol Spectrosc 272:120997. https://doi.org/10.1016/j.saa.2022.120997
169. Yang H, Zhao C, Li R, Shen C, Cai X, Sun L, Luo C, Yin Y (2018) Noninvasive and prospective diagnosis of coronary heart disease with urine using surface-enhanced Raman spectroscopy. Analyst 143(10):2235–2242. https://doi.org/10.1039/c7an02022h
170. Mabbott S, Fernandes SC, Schechinger M, Cote GL, Faulds K, Mace CR, Graham D (2020) Detection of cardiovascular disease associated miR-29a using paper-based microfluidics and surface

enhanced Raman scattering. Analyst 145(3):983–991. https://doi.org/10.1039/c9an01748h
171. Roncarati R, Viviani Anselmi C, Losi MA, Papa L, Cavarretta E, Da Costa Martins P, Contaldi C, Jotti S, Franzone G, Galastri A, Latronico L, Imbriaco MV, Esposito M, De Windt G, Betocchi L, S., Condorelli G (2014) Circulating miR-29a, among other up-regulated microRNAs, is the only biomarker for both hypertrophy and fibrosis in patients with hypertrophic cardiomyopathy. J Am Coll Cardiol 63(9):920–927. https://doi.org/10.1016/j.jacc.2013.09.041
172. John RV, Devasia T, Lukose NM, J., Chidangil S (2022) Micro-raman spectroscopy study of blood samples from myocardial infarction patients. Lasers Med Sci 37(9):3451–3460. https://doi.org/10.1007/s10103-022-03604-1
173. Fang L, Moore XL, Dart AM, Wang LM (2015) Systemic inflammatory response following acute myocardial infarction. J Geriatr Cardiol 12(3):305–312. https://doi.org/10.11909/j.issn.1671-5411.2015.03.020
174. Chon H, Lee S, Yoon SY, Lee EK, Chang SI, Choo J (2014) SERS-based competitive immunoassay of troponin I and CK-MB markers for early diagnosis of acute myocardial infarction. Chem Commun (Camb) 50(9):1058–1060. https://doi.org/10.1039/c3cc47850e
175. Hu C, Ma L, Guan M, Mi F, Peng F, Guo C, Sun S, Wang X, Liu T, Li J (2020) SERS-based magnetic immunoassay for simultaneous detection of cTnI and H-FABP using core-shell nanotags. Anal Methods 12(45):5442–5449. https://doi.org/10.1039/d0ay01564d
176. Thygesen K, Alpert JS, Jaffe AS, Chaitman BR, Bax JJ, Morrow DA, White HD (2018) Fourth Universal Definition of Myocardial Infarction (2018). Circulation, 138(20), e618-e651. https://doi.org/10.1161/cir.0000000000000617
177. Yang X, Zhao Y, Sun L, Qi H, Gao Q, Zhang C (2018) Electrogenerated chemiluminescence biosensor array for the detection of multiple AMI biomarkers. Sens Actuators B 257:60–67
178. Schaap FG, Binas B, Danneberg H, van der Vusse GJ, Glatz JF (1999) Impaired long-chain fatty acid utilization by cardiac myocytes isolated from mice lacking the heart-type fatty acid binding protein gene. Circ Res 85(4):329–337. https://doi.org/10.1161/01.res.85.4.329
179. Agnello L, Bivona G, Novo G, Scazzone C, Muratore R, Levantino P, Bellia C, Sasso L, B., Ciaccio M (2017) Heart-type fatty acid binding protein is a sensitive biomarker for early AMI detection in troponin negative patients: a pilot study. Scand J Clin Lab Invest 77(6):428–432. https://doi.org/10.1080/00365513.2017.1335880
180. Jordanova N, Gyöngyösi M, Khorsand A, Falkensammer C, Zorn G, Wojta J, Anvari A, Huber K (2005) New cut-off values of cardiac markers for risk stratification of angina pectoris. Int J Cardiol 99(3):429–435. https://doi.org/10.1016/j.ijcard.2004.03.003
181. Ohira S, Tanaka H, Harada Y, Minamikawa T, Kumamoto Y, Matoba S, Yaku H, Takamatsu T (2017) Label-free detection of myocardial ischaemia in the perfused rat heart by spontaneous Raman spectroscopy. Sci Rep 7:42401. https://doi.org/10.1038/srep42401
182. Yamamoto T, Minamikawa T, Harada Y, Yamaoka Y, Tanaka H, Yaku H, Takamatsu T (2018) Label-free evaluation of myocardial infarct in surgically excised ventricular myocardium by Raman Spectroscopy. Sci Rep 8(1):14671. https://doi.org/10.1038/s41598-018-33025-6
183. Nishiki-Muranishi N, Harada Y, Minamikawa T, Yamaoka Y, Dai P, Yaku H, Takamatsu T (2014) Label-free evaluation of myocardial infarction and its repair by spontaneous Raman spectroscopy. Anal Chem 86(14):6903–6910. https://doi.org/10.1021/ac500592y
184. Ogawa M, Harada Y, Yamaoka Y, Fujita K, Yaku H, Takamatsu T (2009) Label-free biochemical imaging of heart tissue with high-speed spontaneous Raman microscopy. Biochem Biophys Res Commun 382(2):370–374. https://doi.org/10.1016/j.bbrc.2009.03.028
185. Tombolesi N, Altara R, da Silva GJJ, Tannous C, Zouein FA, Stensløkken KO, Morresi A, Paolantoni M, Booz GW, Cataliotti A, Sassi P (2022) Early cardiac-chamber-specific fingerprints in heart failure with preserved ejection fraction detected by FTIR and Raman spectroscopic techniques. Sci Rep 12(1):3440. https://doi.org/10.1038/s41598-022-07390-2
186. Tolstik E, Ali N, Guo S, Ebersbach P, Möllmann D, Arias-Loza P, Dierks J, Schuler I, Freier E, Debus J, Baba HA, Nordbeck P, Bocklitz T, Lorenz K (2022) CARS imaging advances early diagnosis of Cardiac Manifestation of Fabry Disease. Int J Mol Sci 23(10). https://doi.org/10.3390/ijms23105345
187. Yan Y, Shi R, Yu X, Sun C, Zang W, Tian H (2019) Identification of atrial fibrillation-associated microRNAs in left and right atria of rheumatic mitral valve disease patients. Genes Genet Syst 94(1):23–34. https://doi.org/10.1266/ggs.17-00043
188. Sugiyama K, Marzi J, Alber J, Brauchle EM, Ando M, Yamashiro Y, Ramkhelawon B, Schenke-Layland K, Yanagisawa H (2021) Raman microspectroscopy and Raman imaging reveal biomarkers specific for thoracic aortic aneurysms. Cell Rep Med 2(5):100261. https://doi.org/10.1016/j.xcrm.2021.100261
189. Stanford W, Thompson BH, Weiss RM (1993) Coronary artery calcification: clinical significance and current methods of detection. AJR Am J Roentgenol 161(6):1139–1146. https://doi.org/10.2214/ajr.161.6.8249716
190. Sawada SG, Segar DS, Ryan T, Brown SE, Dohan AM, Williams R, Fineberg NS, Armstrong WF, Feigenbaum H (1991) Echocardiographic detection of coronary artery disease during dobutamine infusion. Circulation 83(5):1605–1614. https://doi.org/10.1161/01.cir.83.5.1605
191. Ho D, Zhao X, Gao S, Hong C, Vatner DE, Vatner SF (2011) Heart Rate and Electrocardiography Monitoring in mice. Curr Protoc Mouse Biol 1:123–139. https://doi.org/10.1002/9780470942390.mo100159
192. Weinschenk SW, Beise RD, Lorenz J (2016) Heart rate variability (HRV) in deep breathing tests and 5-min short-term recordings: agreement of ear photoplethysmography with ECG measurements, in 343 subjects. Eur J Appl Physiol 116(8):1527–1535. https://doi.org/10.1007/s00421-016-3401-3
193. Vasan RS (2006) Biomarkers of cardiovascular disease: molecular basis and practical considerations. Circulation 113(19):2335–2362. https://doi.org/10.1161/circulationaha.104.482570
194. Berthe C, Pierard LA, Hiernaux M, Trotteur G, Lempereur P, Carlier J, Kulbertus HE (1986) Predicting the extent and location of coronary artery disease in acute myocardial infarction by echocardiography during dobutamine infusion. Am J Cardiol 58(13):1167–1172. https://doi.org/10.1016/0002-9149(86)90376-0
195. Low JSY, Thevarajah TM, Chang SW, Goh BT, Khor SM (2020) Biosensing based on surface-enhanced Raman spectroscopy as an emerging/next-generation point-of-care approach for acute myocardial infarction diagnosis. Crit Rev Biotechnol 40(8):1191–1209. https://doi.org/10.1080/07388551.2020.1808582
196. Schilling K, Gao Y, Janve V, Stepniewska I, Landman BA, Anderson AW (2017) Can increased spatial resolution solve the crossing fiber problem for diffusion MRI? NMR Biomed 30(12). https://doi.org/10.1002/nbm.3787
197. Link TM, Majumdar S, Peterfy C, Daldrup HE, Uffmann M, Dowling C, Steinbach L, Genant HK (1998) High resolution MRI of small joints: impact of spatial resolution on diagnostic performance and SNR. Magn Reson Imaging 16(2):147–155. https://doi.org/10.1016/s0730-725x(97)00244-0

198. Nakagawa K, Shimura Y, Fukazawa Y, Nishizaki R, Matano S, Maki H (2021) High resolution IR spectroscopy and imaging based on graphene micro emitters. arXiv Preprint arXiv: 210803327
199. Cao Y, Sun M (2022) Tip-enhanced Raman spectroscopy. Reviews Phys 8:100067. https://doi.org/10.1016/j.revip.2022.100067
200. Bonhommeau S, Lecomte S (2018) Tip-enhanced Raman Spectroscopy: A Tool for Nanoscale Chemical and Structural characterization of Biomolecules. ChemPhysChem 19(1):8–18. https://doi.org/10.1002/cphc.201701067